

# Measurement-altered Ising quantum criticality

Sara Murciano,<sup>1,2,\*</sup> Pablo Sala,<sup>1,2,\*</sup> Yue Liu,<sup>1</sup> Roger S. K. Mong,<sup>3</sup> and Jason Alicea<sup>1,2</sup>

<sup>1</sup>*Department of Physics and Institute for Quantum Information and Matter,  
California Institute of Technology, Pasadena, CA 91125, USA*

<sup>2</sup>*Walter Burke Institute for Theoretical Physics, California Institute of Technology, Pasadena, CA 91125, USA*

<sup>3</sup>*Department of Physics and Astronomy and Pittsburgh Quantum Institute,  
University of Pittsburgh, Pittsburgh, PA 15260, USA*

(Dated: February 10, 2023)

Quantum critical systems constitute appealing platforms for the exploration of novel measurement-induced phenomena due to their innate sensitivity to perturbations. We study the impact of measurement on paradigmatic Ising quantum critical chains using an explicit protocol, whereby correlated ancilla are entangled with the critical chain and then projectively measured. Using a perturbative analytic framework supported by extensive numerical simulations, we demonstrate that measurements can qualitatively alter long-distance correlations in a manner dependent on the choice of entangling gate, ancilla measurement basis, measurement outcome, and nature of ancilla correlations. Measurements can, for example, modify the Ising order-parameter scaling dimension and catalyze order parameter condensation. We derive numerous quantitative predictions for the behavior of correlations in select measurement outcomes, and also identify two strategies for detecting measurement-altered Ising criticality in measurement-averaged quantities. First, averaging the square of the order-parameter expectation value over measurement outcomes retains memory of order parameter condensation germinated in fixed measurement outcomes—even though on average the order parameter itself vanishes. Second, we show that, in certain cases, observables can be averaged separately over measurement outcomes residing in distinct symmetry sectors; we propose that these ‘symmetry-resolved averages’ reveal measurement effects even when considering standard linearly averaged observables. Our framework naturally adapts to more exotic quantum critical points and highlights opportunities for potential experimental realization in Rydberg arrays.

PACS numbers:

## I. INTRODUCTION

Measurements are increasingly viewed as not only a means of probing quantum matter, but also as a resource for generating novel quantum phenomena that may be difficult or impossible to realize solely with unitary evolution. For instance, local measurements that tend to suppress entanglement can compete with entanglement-promoting dynamics—leading to entanglement transitions when these effects compete to a draw [1–3]. Well-studied examples include the volume-to-area law entanglement transition in random Clifford circuits [4–7] and the transition from a critical phase with logarithmic scaling to an area-law phase, e.g., in monitored free fermions [8–10] (see also Refs. 11–25). Measurements additionally provide shortcuts to preparing certain long-range entangled quantum states [26] including wavefunctions associated with topological order [27–31] and quantum criticality [32, 33]. With the advent of analog quantum simulators and noisy intermediate scale quantum hardware, these directions are becoming increasingly experimentally relevant. Indeed, recent experiments have reported signatures of measurement-induced entanglement transitions [34, 35] as well as measurement-assisted preparation of the toric code with a finite-depth quantum

circuit [36].

Despite the impressive progress in this arena, dealing with inherent randomness associated with quantum measurements poses a nontrivial ongoing challenge. Measurement-induced quantum phenomena of interest commonly occur within particular measurement-outcome sectors. Moreover, applying conventional averages of observables over measurement outcomes tends to erase measurement effects altogether. Verification is therefore subtle and can proceed along several possible avenues—e.g., brute-force post-selection [35]; decoding to ‘undo’ randomness injected by measurement using classical post-processing [33], machine learning [37], or active feedback and conditional control [5, 34, 36]; considering non-unitary circuits that are space-time duals to unitary evolution [38–40]; or via cross-entropy benchmarking [41].

Quantum critical systems offer promising venues for exploring nontrivial measurement-induced behavior. First, gaplessness renders such systems inherently sensitive to small perturbations—suggesting that even weak disturbances generated by measurements can yield profound consequences. Second, quantum criticality traditionally manifests in long-distance correlations among *local* observables; one might then anticipate that developing verification protocols here poses a gentler challenge relative to, say, identifying more nuanced entanglement modifications. Pioneering work in Ref. 42 demonstrated that even arbitrarily weak measurements can indeed qualitatively impact long-distance correlations in a

---

\*These authors contributed equally to this work.

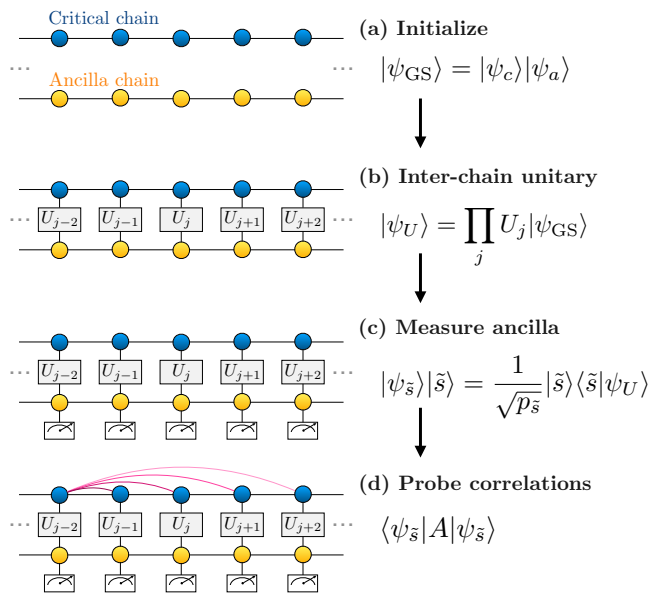


FIG. 1: **Summary of the protocol used to explore measurement-altered Ising criticality.** (a) The upper chain is always initialized into the ground state  $|\psi_c\rangle$  of the critical transverse-field Ising model. The ancilla chain is initialized into the ground state  $|\psi_a\rangle$  of the Ising model either in the paramagnet phase or at criticality. (b) After a unitary that entangles the two chains followed by (c) ancilla measurements, the ancilla chain enters a product state  $|\tilde{s}\rangle$  while the upper chain enters a state  $|\psi_{\tilde{s}}\rangle$  dependent on the measurement outcome  $\tilde{s}$ . (d) Physical operators  $A$  for the top chain are then probed in the state  $|\psi_{\tilde{s}}\rangle$ .

one-dimensional gapless Luttinger liquid, opening up a new frontier of ‘measurement-altered quantum criticality’. More precisely, these authors showed that, in close analogy with the classic Kane-Fisher impurity problem [43], measurement effects can be turned ‘on’ or ‘off’ by varying the Luttinger parameter that characterizes the interaction strength. Reference 42 additionally proposed detection protocols both for post-selected and (unconventionally) measurement-averaged correlators. Subsequently, Ref. 44 associated certain effects of measurement on the Luttinger liquid with an entanglement transition. Measurements have since been further investigated in the context of  $(2+1)$ -dimensional quantum critical points [45]; see also Refs. 46, 47.

In this paper we develop a theory of measurement-altered criticality in paradigmatic one-dimensional Ising quantum critical chains. Ising quantum critical points arise in myriad physical contexts—ranging from Mott insulating spin systems to Rydberg atom arrays—and can also arise in non-interacting model Hamiltonians, thus greatly facilitating analytical and numerical progress. We consider the explicit protocol summarized in Figure 1; to retain nontrivial correlations in the critical chain’s wavefunction, the protocol entangles the critical degrees of freedom with a second chain of correlated ancilla and

then projectively measures the latter. Numerous questions arise here: How are critical correlations modified in specific post-selected measurement outcomes? How do such modifications depend on the choice of entangling gate and ancilla measurement basis used in the protocol? What role do correlations among the ancilla play? And how can one extract nontrivial effects of measurement when averaging over measurement outcomes?

On a technical level, the Ising conformal field theory governing the quantum critical chains we study does not admit any marginal operators that can serve to tune the impact of measurements, unlike the Luttinger liquid setting [42], naively suggesting mundane behavior. On the contrary, we find that measurements can wield exceptionally rich consequences on Ising quantum-critical spin correlations: (i) Scaling dimensions that are otherwise ‘non-negotiable’ in the pristine Ising conformal field theory can become continuously variable in translationally invariant measurement post-selection sectors. (ii) For certain unitary entangling gates in our protocol, coarse-grained spin-spin correlations can be formally obtained from a perturbed Ising conformal field theory for arbitrary measurement outcomes. (iii) Measurements can catalyze order-parameter condensation with a spatial profile dependent on the measurement outcome. Averaging the *square* of the order parameter over measurement outcomes returns a nontrivial result that appears to survive in the thermodynamic limit. (iv) When the ancilla are also initialized into a critical state, we conjecture that measurements can suppress power-law spin-spin correlations altogether while preserving all symmetries. (v) For certain ancilla measurement bases, measurement outcomes can be partitioned into distinct symmetry sectors. We propose that correlations linearly averaged over *particular* symmetry sectors retain nontrivial signatures of measurements. Interestingly, numerical experiments suggest that appropriately normalized differences in such symmetry-resolved averages closely mimic correlations evaluated with uniform post-selection measurement outcomes. We substantiate all of the above using a perturbative analytic framework supplemented by extensive numerical simulations. Collectively, our results shed new light on the interplay between measurements and quantum criticality, and can be potentially tested experimentally in Rydberg arrays [48].

We proceed in Sec. II by first reviewing the microscopic model and continuum theory used throughout, and then detailing our protocol. Section III derives an effective action formalism that incorporates measurement effects into a perturbation to the Ising conformal field action. We critically assess the conditions under which our perturbative action formalism is expected to be valid in Sec. IV. Sections V and VI then examine consequences of our protocol with different ancilla measurement bases. In Sec. VII we develop the formalism of symmetry-resolved measurement averages to propose a post-selection-free scheme for detecting measurement-altered Ising criticality. Finally, Sec. VIII provides a summary and outlook.

## II. SETUP AND PROTOCOL

### A. Review of Ising criticality

Throughout this paper we explore the effect of measurements on an Ising quantum critical point realized microscopically in the canonical transverse field Ising model,

$$H = \sum_j (-J Z_j Z_{j+1} - h X_j). \quad (1)$$

Here  $Z_j$  and  $X_j$  are Pauli operators acting on site  $j$  of a chain with periodic boundary conditions (unless specified otherwise). Additionally, we assume ferromagnetic interactions,  $J > 0$ , and a positive transverse field,  $h > 0$ . Equation (1) preserves both time reversal symmetry  $\mathcal{T}$ —which leaves  $X_j$  and  $Z_j$  invariant but enacts complex conjugation—and global  $\mathbb{Z}_2$  spin flip symmetry generated by  $G = \prod_j X_j$ . At  $h > J$ , the system realizes a symmetry-preserving paramagnetic phase. For  $h < J$ , a ferromagnetic phase emerges, characterized by a non-zero order parameter  $\langle Z_j \rangle \neq 0$  that indicates spontaneously broken  $\mathbb{Z}_2$  symmetry. The paramagnetic and ferromagnetic phases are related under a duality transformation that interchanges  $J \leftrightarrow h$ .

Ising criticality appears at the self-dual point  $J = h$ —to which we specialize hereafter. The low-energy critical theory is most easily accessed via a Jordan-Wigner transformation to Majorana fermion operators

$$\gamma_{Aj} = \left( \prod_{k < j} X_k \right) Z_j, \quad \gamma_{Bj} = \left( \prod_{k < j} X_j \right) i X_j Z_j. \quad (2)$$

In this basis the  $J = h$  Hamiltonian becomes

$$H_c = iJ \sum_j (\gamma_{Aj+1} - \gamma_{Aj}) \gamma_{Bj}. \quad (3)$$

Focusing on long-wavelength Fourier components of  $\gamma_{Aj}$  and  $\gamma_{Bj}$ , which comprise the important degrees of freedom at criticality, yields the continuum Hamiltonian  $\mathcal{H}_c = iv \int_x (\partial_x \gamma_A) \gamma_B$  with  $v \propto J$ . Upon changing basis to  $\gamma_A = \gamma_R + \gamma_L$  and  $\gamma_B = \gamma_R - \gamma_L$ , we arrive at

$$\mathcal{H}_c = -iv \int_x (\gamma_R \partial_x \gamma_R - \gamma_L \partial_x \gamma_L), \quad (4)$$

which describes kinetic energy for right- and left-moving Majorana fermions  $\gamma_R$  and  $\gamma_L$ .

Equation (4) corresponds to an Ising conformal field theory (CFT) with central charge  $c = 1/2$  [49]. The Ising CFT exhibits three primary fields: the identity  $\mathbb{1}$ , the ‘spin field’  $\sigma$  (scaling dimension  $\Delta_\sigma = 1/8$ ), and the ‘energy field’  $\varepsilon$  (dimension  $\Delta_\varepsilon = 1$ ). The spin field is odd under  $\mathbb{Z}_2$  symmetry and represents the continuum limit of the ferromagnetic order parameter. Consequently, only correlators containing an even number of spin fields can

be non-zero at criticality. For instance, one- and two-point spin-field correlators read

$$\langle \sigma(x) \rangle = 0, \quad \langle \sigma(x) \sigma(x') \rangle \sim \frac{1}{|x - x'|^{1/4}}. \quad (5)$$

The energy field is a composite of right- and left-movers,  $\varepsilon = i\gamma_R \gamma_L$ ; this field is odd under duality and hence represents a perturbation that moves the system off of criticality. The operator product expansion for two fields at different points determine the following fusion rules:

$$\begin{cases} \sigma \times \sigma = \mathbb{1} + \varepsilon, \\ \varepsilon \times \varepsilon = \mathbb{1}, \\ \sigma \times \varepsilon = \sigma. \end{cases} \quad (6)$$

Local microscopic spin operators admit straightforward expansions in terms of the above CFT fields and their descendants. In particular, we have

$$Z_j \sim \sigma + \dots \quad (7)$$

$$X_j - \langle X \rangle \sim \varepsilon + \dots, \quad (8)$$

where the ellipses denote fields with subleading scaling dimension. Equation (7) follows from  $\mathbb{Z}_2$  symmetry together with translation invariance of the ferromagnetic phase (for the antiferromagnetic case,  $J < 0$ , an additional  $(-1)^j$  factor would appear on the right side). In Eq. (8),  $\langle X \rangle$  denotes the (position-independent) ground-state expectation value of  $X_j$ —which is generically non-zero due to the transverse field. In the thermodynamic limit at criticality one finds  $\langle X \rangle = 2/\pi$ . Subtracting off this expectation value from the left-hand side removes terms proportional to the identity field on the right-hand side. One can understand the appearance of  $\varepsilon$  in Eq. (8) by noting that perturbing the microscopic Hamiltonian with a term  $\propto \sum_j X_j$  moves the system off of criticality, corresponding to the generation of the energy field in the continuum theory. (The same conclusion follows by expressing  $X_j$  in terms of Majorana fermions and taking the continuum limit [64].)

With the aid relations like Eqs. (7) and (8), standard techniques relate ground-state expectation values of microscopic operators to averages of CFT fields expressed in path-integral language. We illustrate the approach in a way that will be useful for exploring the influence of measurements in Sec. III B. The ground-state expectation value of a microscopic operator  $A$  in the critical chain’s ground state  $|\psi_c\rangle$ ,

$$\langle A \rangle = \langle \psi_c | A | \psi_c \rangle, \quad (9)$$

can always be expressed as

$$\langle A \rangle = \lim_{\beta \rightarrow \infty} \frac{1}{Z} \text{Tr} \left\{ e^{-\beta H_c/2} A e^{-\beta H_c/2} \right\}. \quad (10)$$

The  $e^{-\beta H_c/2}$  factors in the numerator project away excited state components from the bra and ket in each

element of the trace, and the partition function  $Z = \lim_{\beta \rightarrow \infty} \text{Tr}\{e^{-\beta H_c}\}$  in the denominator ensures proper normalization. Next we take the continuum limit of both sides:

$$\langle A \rangle \sim \langle \mathcal{A} \rangle = \lim_{\beta \rightarrow \infty} \frac{1}{Z} \text{Tr}\left\{e^{-\beta \mathcal{H}_c/2} \mathcal{A} e^{-\beta \mathcal{H}_c/2}\right\}. \quad (11)$$

Calligraphic fonts indicate low-energy expansions of the corresponding quantities in Eq. (10). For instance, if  $A = Z_j Z_{j'}$ , then Eq. (7) gives  $\mathcal{A} = \sigma(x_j) \sigma(x_{j'})$  for  $x_i$  a continuum coordinate corresponding to site  $i$ . Finally, Trotterizing the exponentials and inserting resolutions of identity in the fermionic coherent state basis yields

$$\langle \mathcal{A} \rangle = \lim_{\beta \rightarrow \infty} \frac{1}{Z} \int \mathcal{D}\gamma_R \mathcal{D}\gamma_L e^{-\mathcal{S}_c} \mathcal{A}(\tau = 0) \quad (12)$$

with the Euclidean Ising CFT action

$$\mathcal{S}_c = \int_x \int_{-\beta/2}^{\beta/2} d\tau [\gamma_R(\partial_\tau - iv\partial_x)\gamma_R + \gamma_L(\partial_\tau + iv\partial_x)\gamma_L]. \quad (13)$$

Note that in our convention imaginary time  $\tau$  runs from  $-\beta/2$  to  $+\beta/2$  with  $\beta \rightarrow \infty$ ; the operator ordering in Eq. (11) then naturally gives  $\mathcal{A}$  evaluated at  $\tau = 0$  in Eq. (12).

## B. Protocol

We now introduce a second transverse-field Ising chain, composed of ancilla spins, that will enable us to enact an extensive set of projective measurements that partially preserve the nontrivial entanglement of our critical Ising chain. Specifically, the ancilla Hamiltonian is

$$H_{\text{anc}} = \sum_j (-J_{\text{anc}} \tilde{Z}_j \tilde{Z}_{j+1} - h_{\text{anc}} \tilde{X}_j), \quad (14)$$

where  $\tilde{Z}_j$  and  $\tilde{X}_j$  are Pauli operators for the ancilla spins and we assume  $J_{\text{anc}}, h_{\text{anc}} > 0$ . Throughout we work in the regime  $h_{\text{anc}} \geq J_{\text{anc}}$ —i.e., the ancilla are either critical or realize the gapped paramagnetic phase, so that the spin-flip symmetry generated by  $\tilde{G} = \prod_j \tilde{X}_j$  is always preserved in the ground state.

Inspired by Ref. 42, we consider the following protocol (see Figure 1 for a summary):

(a) Initialize the system into the wavefunction

$$|\psi_{\text{GS}}\rangle = |\psi_c\rangle |\psi_a\rangle, \quad (15)$$

where  $|\psi_c\rangle$  is the ground state of the top (critical) chain and  $|\psi_a\rangle$  is the ground state of the bottom (ancilla) chain.

(b) Apply a unitary gate  $U_j$  to each pair of adjacent sites from the critical and ancilla chains, sending

$$|\psi_{\text{GS}}\rangle \rightarrow |\psi_U\rangle = \left( \prod_j U_j \right) |\psi_c\rangle |\psi_a\rangle. \quad (16)$$

The unitaries we apply generally consist of single-spin ancilla rotations followed by a two-spin entangling gate, and are always implemented in a translationally invariant manner.

(c) Projectively measure all ancilla spins in some fixed basis, e.g.,  $\tilde{Z}$  or  $\tilde{X}$ , yielding measurement outcome

$$\tilde{s} \equiv \{\tilde{s}_j\} \quad (17)$$

with  $\tilde{s}_j \in \pm 1$ . The wavefunction correspondingly collapses to  $|\psi_{\tilde{s}}\rangle |\tilde{s}\rangle$ ; here  $|\psi_{\tilde{s}}\rangle$  denotes the post-measurement state for the top chain, which depends on the outcome  $\tilde{s}$ . More precisely, this step sends

$$\begin{aligned} |\psi_U\rangle &\xrightarrow{\text{measure}} |\psi_{\tilde{s}}\rangle |\tilde{s}\rangle \\ &= \frac{1}{\sqrt{p_{\tilde{s}}}} \left( \prod_j |\tilde{s}_j\rangle \langle \tilde{s}_j| U_j \right) |\psi_c\rangle |\psi_a\rangle, \end{aligned} \quad (18)$$

where the normalization

$$p_{\tilde{s}} = \langle \psi_a | \langle \psi_c | \left( \prod_j U_j^\dagger |\tilde{s}_j\rangle \langle \tilde{s}_j| U_j \right) |\psi_c\rangle |\psi_a\rangle \quad (19)$$

specifies the probability for obtaining measurement outcome  $\tilde{s}$ .

(d) Probe correlations on the top chain for the post-measurement state  $|\psi_{\tilde{s}}\rangle$ .

Inspection of Eq. (18) reveals that the ancilla measurements can nontrivially impact correlations in the critical chain only if the measurement basis and unitaries are chosen such that  $[|\tilde{s}_j\rangle \langle \tilde{s}_j|, U_j] \neq 0$  [65]. Even in this case, however, extracting measurement-induced changes in correlations poses a subtle problem. For an arbitrary critical-chain observable  $A$ , performing a standard average of  $\langle \psi_{\tilde{s}} | A | \psi_{\tilde{s}} \rangle$  over ancilla measurement outcomes simply recovers the expectation value  $\langle \psi_U | A | \psi_U \rangle$  taken in the pre-measurement state. Indeed, using Eqs. (16) and (18) yields

$$\begin{aligned} \sum_{\tilde{s}} p_{\tilde{s}} \langle \psi_{\tilde{s}} | A | \psi_{\tilde{s}} \rangle &= \sum_{\tilde{s}} \langle \psi_U | \left( \prod_j |\tilde{s}_j\rangle \langle \tilde{s}_j| \right) \\ &\times A \left( \prod_j |\tilde{s}_j\rangle \langle \tilde{s}_j| \right) | \psi_U \rangle \\ &= \sum_{\tilde{s}} \langle \psi_U | \left( \prod_j |\tilde{s}_j\rangle \langle \tilde{s}_j| \right) A | \psi_U \rangle = \langle \psi_U | A | \psi_U \rangle. \end{aligned} \quad (20)$$

The second equality follows from the fact that the projectors  $|\tilde{s}_j\rangle \langle \tilde{s}_j|$  commute with  $A$  (because they act on different chains) and square to themselves, while the third follows upon removing a resolution of the identity for the ancilla chain.

Our protocol can be understood as a particular physical implementation of generalized measurement protocols that combine additional degrees of freedom, a unitary entangling transformation, and projective measurements (see, e.g., Ref. 50). Notably, it allows us to assess how quantum correlations among the ancilla, tunable via the ratio  $h_{\text{anc}}/J_{\text{anc}}$ , impact the measurement-induced changes in the critical chain's properties. Let us make this connection more explicit. The post-measured state  $|\psi_{\tilde{s}}\rangle$  given in Eq. (18) can be written as

$$|\psi_{\tilde{s}}\rangle = \frac{1}{\sqrt{p_{\tilde{s}}}} M_{\tilde{s}} |\psi_c\rangle, \quad (21)$$

where, given measurement outcome  $\tilde{s}$ ,  $M_{\tilde{s}} \equiv \langle \tilde{s} | \prod_j U_j | \psi_a \rangle$  denotes the measurement operator acting on the critical chain. The full set of measurement operators satisfy the completeness relation  $\sum_{\tilde{s}} M_{\tilde{s}}^\dagger M_{\tilde{s}} = \mathbb{1}_c$ . If  $|\psi_a\rangle$  was a product state, then we could factorize  $M_{\tilde{s}} = \prod_j M_{\tilde{s}_j}$  in terms of on-site measurement operators  $M_{\tilde{s}_j}$ . However, for nontrivially entangled  $|\psi_a\rangle$ —which we always consider below—this exact factorization no longer holds, though an approximate factorization can nevertheless suffice to capture the essential influence of measurement, depending on the precise form of  $M_{\tilde{s}}$  and the range of ancilla correlations. We return to this point in Sec. VIII.

Subsequent sections investigate the protocol with different classes of unitaries and measurement bases using a combination of field-theoretic and numerical tools. The latter combine covariant-matrix techniques for Gaussian states (explained in Appendix A) when characterizing a single chain; exact diagonalization (ED) to exactly evaluate averages over measurement outcomes; and tensor network methods [51], using the density matrix renormalization group (DMRG) method [52] and its infinite variant (iDMRG) [53] to evaluate correlations on specific measurement outcomes. As a prerequisite, next we develop a perturbative formalism that we use extensively to distill measurement effects into a perturbation to the Ising CFT action.

### III. EFFECTIVE ACTION FORMALISM

Table I lists the four classes of unitaries  $U_j$  that we examine, together with the corresponding ancilla measurement basis taken for each case. In the second column,  $\langle X \rangle = \langle \psi_c | X_j | \psi_c \rangle$  as defined previously,  $C$  is a constant, and  $u$  characterizes the strength of the unitary—i.e., how far  $U_j$  is from the identity. As we will see later, the symmetry of  $U_j$  depends on whether  $C = 0$  or  $C \neq 0$  in a manner that qualitatively affects critical-chain correlations after measurement. Throughout our analytical treatment, we assume small  $u \ll 1$  that does not scale with system size. Our goal in Sec. III A is to recast the post-measurement state in the form

$$|\psi_{\tilde{s}}\rangle = \frac{1}{\sqrt{\mathcal{N}}} U' e^{-H_m/2} |\psi_c\rangle. \quad (22)$$

Case	Unitary $U_j$	Ancilla measurement basis
I	$\exp[iu(X_j - \langle X \rangle)\tilde{X}_j]$	$\tilde{Z}$
II	$\exp[iu(Z_j - C)\tilde{X}_j]$	$\tilde{Z}$
III	$\exp[iu(X_j - \langle X \rangle)\tilde{Z}_j]$	$\tilde{X}$
IV	$\exp[iu(Z_j - C)\tilde{Z}_j]$	$\tilde{X}$

TABLE I: Four classes of unitaries used in our protocols, along with the corresponding ancilla measurement basis. In cases II and IV,  $C$  is a constant that controls whether or not the post-measurement state  $|\psi_{\tilde{s}}\rangle$  preserves global spin-flip symmetry for the critical chain.

Here  $U'$  is a unitary operator acting solely on the critical chain, while  $H_m$  is a Hermitian operator, organized systematically in powers of  $u$ , that encodes the non-unitary change in  $|\psi_U\rangle$  imposed by the measurement. One can view this representation of  $|\psi_{\tilde{s}}\rangle$  as arising from a polar decomposition of the measurement operator  $M_{\tilde{s}}$  in Eq. (21), up to an overall constant (dependent on  $\tilde{s}$ ) that is absorbed into the normalization factor  $\mathcal{N}$ . Section III B uses the form in Eq. (22) to develop a continuum-limit CFT framework for characterizing observables given a fixed ancilla measurement outcome.

#### A. Perturbative framework

All four unitaries in Table I take the form

$$U_j = e^{iu(O_j - \theta)\tilde{O}_j}. \quad (23)$$

The constant  $\theta$  is either  $\langle X \rangle$  (cases I, III) or  $C$  (cases II, IV), while  $O_j$  and  $\tilde{O}_j$  denote Pauli matrices that respectively act on the critical chain and ancilla. Additionally, the ancilla measurement basis is always orthogonal to  $\tilde{O}_j$ ; hence if measurement projects ancilla site  $j$  to  $|\tilde{s}_j\rangle$ , then  $\tilde{O}_j$  simply flips that measured spin:  $\tilde{O}_j |\tilde{s}_j\rangle = |-\tilde{s}_j\rangle$ . For the unitary in Eq. (23), we can then use properties of Pauli operators to express the post-measurement state defined in Eq. (18) as

$$|\psi_{\tilde{s}}\rangle = \frac{1}{\sqrt{p_{\tilde{s}}}} \left\{ \left[ \prod_j (C_j \langle \tilde{s}_j | + S_j \langle -\tilde{s}_j |) \right] |\psi_a\rangle \right\} |\psi_c\rangle. \quad (24)$$

Equation (24) uses the short-hand notation

$$C_j = \cos[u(O_j - \theta)], \quad S_j = i \sin[u(O_j - \theta)], \quad (25)$$

which satisfy standard trigonometric identities even including the Pauli operators in the arguments.

Observe that multiplying all elements in the product from Eq. (24) yields a sum of terms with anywhere from  $N_f = 0$  to  $N$  flipped ancilla spins ( $N$  is the total number of ancilla sites), and that these flipped spins can occur at

arbitrary sites  $i_1 < i_2 < \dots < i_{N_f}$ . Let  $|\tilde{s}(i_1, \dots, i_{N_f})\rangle$  be the state with  $N_f$  flipped ancilla spins at these sites, and let  $F(i_1, \dots, i_{N_f})$  denote a product of  $C_j$ 's for the unflipped sites and  $S_j$ 's for the flipped sites. For example,

$$\begin{aligned} |\tilde{s}(i_1, i_2)\rangle &= \tilde{O}_{i_1} \tilde{O}_{i_2} |\tilde{s}\rangle, \\ F(i_1, i_2) &= C_1 \dots C_{i_1-1} S_{i_1} C_{i_1+1} \dots C_{i_2-1} S_{i_2} C_{i_2+1} \dots \end{aligned} \quad (26)$$

We can then explicitly write

$$\begin{aligned} |\psi_{\tilde{s}}\rangle &= \frac{1}{\sqrt{p_{\tilde{s}}}} \sum_{N_f=0}^N \sum_{i_1 < i_2 < \dots < i_{N_f}} \langle \tilde{s}(i_1, \dots, i_{N_f}) | \psi_a \rangle \\ &\quad \times F(i_1, \dots, i_{N_f}) |\psi_c\rangle \end{aligned} \quad (27)$$

which, en route to the form in Eq. (22), can be trivially re-expressed as

$$\begin{aligned} |\psi_{\tilde{s}}\rangle &= \frac{1}{\sqrt{p_{\tilde{s}}}} \exp \left\{ \ln \left[ \langle \tilde{s} | \psi_a \rangle F_0 + \sum_i \langle \tilde{s}(i) | \psi_a \rangle F(i) \right. \right. \\ &\quad \left. \left. + \sum_{i_1 < i_2} \langle \tilde{s}(i_1, i_2) | \psi_a \rangle F(i_1, i_2) + \dots \right] \right\} |\psi_c\rangle \end{aligned} \quad (28)$$

with  $F_0 \equiv C_1 \dots C_N$ .

Suppose now that  $\langle \tilde{s} | \psi_a \rangle$  is non-zero. In this case we can factor out the first term in the log from Eq. (28) to obtain, after some manipulation and absorbing an  $\tilde{s}$ -dependent constant into a new normalization factor  $\mathcal{N}$ ,

$$\begin{aligned} |\psi_{\tilde{s}}\rangle &= \frac{1}{\sqrt{\mathcal{N}}} e^{-H_{\text{temp}}/2} |\psi_c\rangle, \\ H_{\text{temp}} &= -2 \ln \left[ 1 + \sum_i a(i) T_i \right. \\ &\quad \left. + \sum_{i_1 < i_2} a(i_1, i_2) T_{i_1} T_{i_2} + \dots \right] - 2 \sum_i \ln(C_i). \end{aligned} \quad (29)$$

In the second and third lines we introduced the quantities

$$a(i_1, \dots, i_{N_f}) = \frac{\langle \tilde{s}(i_1 \dots i_{N_f}) | \psi_a \rangle}{\langle \tilde{s} | \psi_a \rangle}, \quad T_i = C_i^{-1} S_i. \quad (31)$$

At this point one can expand  $H_{\text{temp}}$  to the desired order in  $u \ll 1$ . To proceed it is convenient to decompose  $H_{\text{temp}}$  via

$$H_{\text{temp}} = -2iH' + H_m, \quad (32)$$

where  $H', H_m$  are commuting Hermitian operators;  $U' = e^{iH'}$  is the unitary transformation from Eq. (22) while  $H_m$  contains the crucial non-unitary effects from measurement. Upon absorbing constants into the normaliza-

tion  $\mathcal{N}$ , to  $O(u^2)$  we obtain

$$\begin{aligned} H' &= u \sum_j a(j) (O_j - \langle O \rangle), \\ H_m &= u^2 \sum_j m_j (O_j - \langle O \rangle) \\ &\quad + u^2 \sum_{j \neq k} V_{jk} (O_j - \langle O \rangle) (O_k - \langle O \rangle). \end{aligned} \quad (33)$$

For later convenience we have organized the contributions in terms of  $O_j - \langle O \rangle$ , where  $\langle O \rangle = \langle \psi_c | O_j | \psi_c \rangle$  is the expectation value of  $O_j$  in the initialized state, prior to applying the unitary and measuring. Equation (34) contains coefficients

$$V_{jk} = a(j, k) - a(j)a(k) \quad (35)$$

$$m_j = -2\theta[1 - a(j)^2] + 2(\langle O \rangle - \theta) \sum_{k \neq j} V_{jk}. \quad (36)$$

We stress that  $U' = e^{iH'}$  factorizes into a product of operators acting on a single site  $j$ —i.e., one can always decompose  $U' = \prod_j U'_j$  at order  $O(u^2)$ —whereas  $e^{-H_m/2}$  admits no such factorization due to the  $V_{jk}$  term. The leading corrections to  $H'$  and  $H_m$  arise at  $O(u^3)$  and  $O(u^4)$ , respectively.

The preceding derivation assumed  $\langle \tilde{s} | \psi_a \rangle \neq 0$ , which holds provided measurement outcome  $\tilde{s}$  can arise even at  $u = 0$ , where the unitary applied in our protocol reduces to the identity. As we will see below, however, symmetry can constrain  $\langle \tilde{s} | \psi_a \rangle = 0$  for a class of  $\tilde{X}$ -basis measurement outcomes. In the latter case our expansion for  $H_m$  and  $H'$  breaks down [as evidenced by the vanishing denominator in  $a(i_1, \dots, i_{N_f})$  from Eq. (31)]. Nevertheless, even without an action-based framework, in Sec. VII we will use a non-perturbative technique to constrain correlations resulting from such measurement outcomes. For now we neglect this case and continue to assume  $\langle \tilde{s} | \psi_a \rangle \neq 0$  in the remainder of this section.

## B. Continuum limit

Using Eq. (22), the expectation value of a general critical-chain observable  $A$  in the state  $|\psi_{\tilde{s}}\rangle$  associated with measurement outcome  $\tilde{s}$  reads

$$\langle A \rangle_{\tilde{s}} = \frac{1}{\mathcal{N}} \langle \psi_c | e^{-H_m/2} A_{U'} e^{-H_m/2} | \psi_c \rangle, \quad (37)$$

where  $A_{U'} = U'^{\dagger} A U'$ . The numerator on the right-hand side of Eq. (37) has the same form as the right side of Eq. (9), but with  $A \rightarrow e^{-H_m/2} A_{U'} e^{-H_m/2}$  as a consequence of the unitary and measurement applied in our protocol. Furthermore, the normalization constant  $\mathcal{N} = \langle \psi_c | e^{-H_m} | \psi_c \rangle$  also has the form of Eq. (9) with  $A \rightarrow e^{-H_m}$ . Following exactly the logic below Eq. (9) for

both the numerator and demoninator leads to the continuum expansion

$$\begin{aligned} \langle A \rangle_{\tilde{s}} &\sim \langle \mathcal{A} \rangle_{\tilde{s}} \\ &= \lim_{\beta \rightarrow \infty} \frac{1}{\mathcal{Z}'} \int \mathcal{D}\gamma_R \mathcal{D}\gamma_L e^{-(\mathcal{S}_c + \mathcal{S}_m)} \mathcal{A}_{U'}(\tau = 0) \end{aligned} \quad (38)$$

that generalizes Eq. (12). The new partition function is

$$\mathcal{Z}' = \int \mathcal{D}\gamma_R \mathcal{D}\gamma_L e^{-(\mathcal{S}_c + \mathcal{S}_m)}. \quad (39)$$

Most crucially, the Ising CFT action  $\mathcal{S}_c$  from Eq. (13) has been appended with a ‘defect line’ acting at all positions  $x$  but only at imaginary time  $\tau = 0$ , encoded through

$$\mathcal{S}_m = \int_x \mathcal{H}_m(\tau = 0) \quad (40)$$

with  $\mathcal{H}_m$  the continuum expansion of  $H_m$ . The explicit form of the defect line action  $\mathcal{S}_m$  depends on the unitary  $U$  and measurement basis, and will be explored in depth in Secs. V and VI for cases I through IV in Table I. Specifically, we seek to understand its impact on observables  $\mathcal{A}_{U'}$ —which are also evaluated at  $\tau = 0$  in the path integral description. (Technically,  $\mathcal{A}_{\tilde{U}}$  is sandwiched between two factors of  $e^{-\mathcal{S}_m/2}$  evaluated at slightly different imaginary times. We approximated this combination as  $\mathcal{A}_{\tilde{U}} e^{-\mathcal{S}_m}$  since the leading scaling behavior is unchanged by this rewriting.) It is important, however, to first understand the conditions under which the perturbative expansion developed above is expected to be controlled. To this end we now study the properties of the  $V_{jk}$  and  $m_j$  couplings in Eq. (34).

#### IV. PROPERTIES OF $V_{jk}$ AND $m_j$ COUPLINGS

In general, both  $V_{jk}$  and  $m_j$  vary nontrivially with the site indices in a manner dependent on the measurement outcome. The couplings  $V_{jk}$  control the interaction range in  $H_m$ , and exhibit a structure reminiscent of a connected correlator. That is,  $V_{jk}$  specifies how the overlap between the initial ancilla wavefunction and the measured state changes under a *correlated* flip of spins at sites  $j, k$ . It is thus natural to expect that  $V_{jk}$  statistically averaged over measurement outcomes, denoted  $\bar{V}_{jk}$ , decays with  $|j - k|$ —either exponentially if the ancilla are initialized into the ground state of the gapped paramagnetic phase, or as a power-law if the ancilla are critical. We confirm this expectation below. The statistically averaged  $m_j$  coefficients, denoted  $\bar{m}_j$ , would then not suffer from a divergence in the presence of the  $\sum_{k \neq j} V_{jk}$  term in Eq. (36), so long as  $\bar{V}_{jk}$  decays faster than  $1/|j - k|$  (which does not always hold as we will see later).

For a *particular* measurement outcome  $\tilde{s}$ , control of the expansion leading to  $H_m$  in the previous subsection requires, at a minimum, that  $V_{jk}$  and  $m_j$  for this outcome are similarly well-behaved. For example, if the amplitude of  $m_j$  for a particular  $\tilde{s}$  grows with system size  $N$ ,

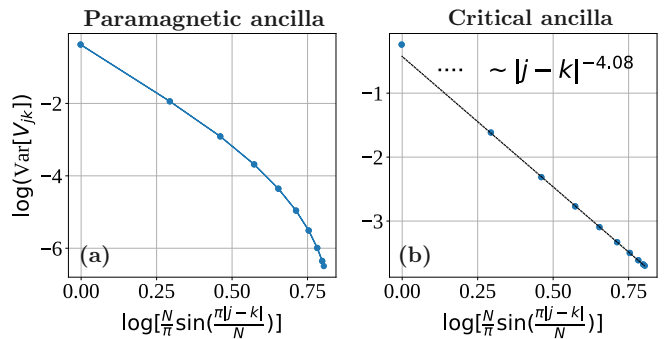


FIG. 2: (Color online). **Variance of  $V_{jk}$  for  $\tilde{Z}$ -basis measurements.** Panels (a) and (b) respectively correspond to paramagnetic and critical ancilla. The variance decays exponentially with  $|j - k|$  in the former but decays approximately as  $|j - k|^{-4}$  in the latter. Data were obtained using the methods in Appendix A with a system size  $N = 20$ .

then  $u \ll 1$  does not suffice to control the expansion (assuming that  $u$  does not also scale with system size). Additionally, if  $V_{jk}$  for a given  $\tilde{s}$  does not decay to zero with  $|j - k|$ , then the correspondingly infinite-range interaction in Eq. (34) makes the expansion suspect. Thus it is crucial to quantify not only the mean but also the variances  $\text{Var}(V_{jk})$  and  $\text{Var}(m_j)$  of the couplings in  $H_m$ —which will inform which set of measurement outcomes we analyze later on. Next, we address this problem for the four classes of unitaries/ancilla measurement bases listed in Table I.

In all four cases we statistically average using the  $u = 0$  distribution for the ancilla measurement outcomes,

$$p_{\tilde{s}} = \langle \tilde{s} | \psi_a \rangle^2 \langle \psi_c | e^{-H_m} | \psi_c \rangle \sim \langle \tilde{s} | \psi_a \rangle^2 \equiv p_{\tilde{s}}^{(0)}, \quad (41)$$

since  $m_j$  and  $V_{jk}$  already come with  $u^2$  prefactors. In Eq. (41) and many places below, we take advantage of the fact that the overlaps  $\langle \tilde{s} | \psi_a \rangle$  are non-negative, which follows because the transverse-field Ising model [Eq. (14)] is *stoquastic* [54]. That is, on a given computational basis state  $|v\rangle$ —in this case the  $z$  or  $x$  local basis— $\langle v | H_{\text{anc}} | w \rangle \leq 0$  for  $v \neq w$ , from which it follows that  $\langle v | \psi_a \rangle \geq 0$  for arbitrary basis states  $v$ . Hence, all elements  $a(i_1, \dots, i_{N_F})$  from Eq. (31) are also non-negative. Finally, since the fermionized  $H_{\text{anc}}$  is quadratic in Majorana fermion fields, we exploit the Gaussianity of both  $|\psi_a\rangle$  and  $|\tilde{s}\rangle$  to evaluate the elements  $a(i_1, \dots, i_{N_F})$  using covariance-matrix techniques; see Appendix A. These tools, along with standard results for transverse-field Ising chain correlators, allow us to compute the probabilities  $p_{\tilde{s}}^{(0)}$  as well as the mean and variance of  $m_j$  and  $V_{jk}$  below.

### A. $\tilde{Z}$ measurement basis

When the ancilla are measured in the  $\tilde{Z}$  basis, the mean and variance of  $V_{jk}$  evaluate to

$$\bar{V}_{jk} = \sum_{\tilde{s}} p_{\tilde{s}}^{(0)} V_{jk} = 0 \quad (42)$$

$$\begin{aligned} \text{Var}(V_{jk}) &= \sum_{\tilde{s}} p_{\tilde{s}}^{(0)} V_{jk}^2 - (\bar{V}_{jk})^2 \\ &= 1 + \sum_{\tilde{s}} p_{\tilde{s}}^{(0)} a(j)a(k)[a(j)a(k) - 2a(j, k)]. \end{aligned} \quad (43)$$

Figure 2 illustrates  $\text{Var}(V_{jk})$  versus  $|j-k|$  determined numerically at  $N = 20$ , for both (a) paramagnetic ancilla and (b) critical ancilla ( $h_{\text{anc}}/J_{\text{anc}} = 1$ ). In Figure 2(a) and all subsequent simulations that use paramagnetic ancilla, we take  $h_{\text{anc}}/J_{\text{anc}} = 1.5$ . Additionally, when using periodic boundary conditions we present numerical results for correlations as a function of  $\frac{N}{\pi} \sin\left(\frac{\pi|j-k|}{N}\right)$  to reduce finite-size effects [48]. The variances in Figure 2 clearly tend to zero at large  $|j-k|$ , exponentially with paramagnetic ancilla and as a power-law (with decay exponent  $\approx 4$ ) for critical ancilla. This decay suggests that typical  $\tilde{Z}$ -basis measurement outcomes yield well-behaved, decaying interactions in the second line of Eq. (34).

Due to the dependence on  $\theta$  and  $\langle O \rangle$  in Eq. (36), the mean and variance of  $m_j$  depend on the unitary applied in the protocol. For case I in Table I we have  $\theta = \langle O \rangle = \langle X \rangle = 2/\pi$  while case II corresponds to  $\theta = C$ ,  $\langle O \rangle = 0$ . For these cases we find

$$\bar{m}_j^{\text{I}} = \bar{m}_j^{\text{II}} = 0 \quad (44)$$

$$\text{Var}(m_j^{\text{I}}) = 4\langle X \rangle^2 \left[ -1 + \sum_{\tilde{s}} p_{\tilde{s}}^{(0)} a(j)^4 \right] \quad (45)$$

$$\text{Var}(m_j^{\text{II}}) = 4C^2 \left\{ -1 + \sum_{\tilde{s}} p_{\tilde{s}}^{(0)} \left[ a(j)^2 - \sum_{k \neq j} V_{jk} \right]^2 \right\}. \quad (46)$$

Figure 3 illustrates the numerically evaluated standard deviation  $\sqrt{\text{Var}(m_j^{\text{I,II}})}$  versus inverse system size  $1/N$ , again for both paramagnetic and critical ancilla. (For case II we assume  $C \neq 0$  here, since otherwise  $m_j$  simply vanishes.) With paramagnetic ancilla, the standard deviation clearly converges at large  $N$  to a finite value for both case I and case II. With critical ancilla, in both cases the standard deviation is modestly larger for the system sizes shown, albeit showing *very* slow, potentially saturating, growth with  $N$ . Although here we can not ascertain the trend for the thermodynamic limit, we expect that for experimentally relevant  $N$  values the variance of  $m_j$  remains of the same order of magnitude as for the paramagnetic case.

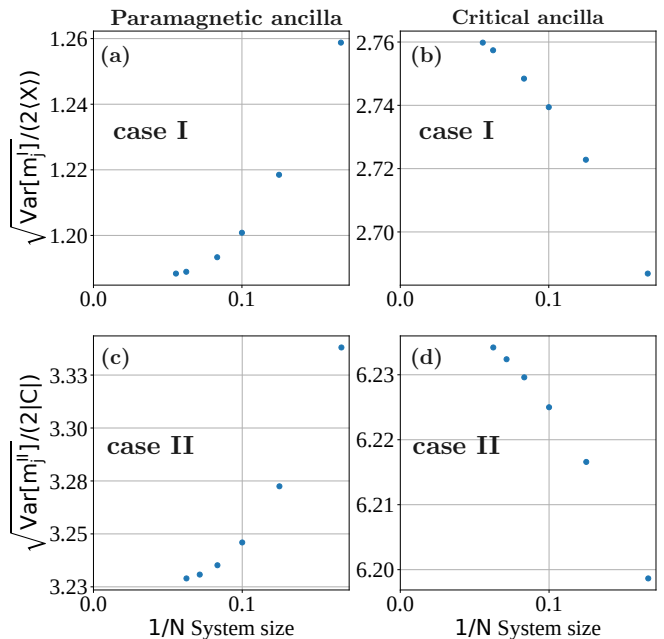


FIG. 3: (Color online). **Standard deviation of  $m_j$  for  $\tilde{Z}$ -basis measurements.** For paramagnetic ancilla (panels (a, c)) in either case I or case II, the standard deviation decreases with  $N$ , with the trend suggesting saturation to a finite value in the thermodynamic limit. With critical ancilla (panels (b, d)) the standard deviation increases extremely slowly with  $N$  in both cases but remains comparable to the values with paramagnetic ancilla. Data were obtained using results from Appendix A.

The behavior of the variances discussed above suggests that, at least for paramagnetic ancilla, any typical string outcome yields a well-behaved defect-line action amenable to our perturbative formalism. To support this expectation, we illustrate  $V_{jk}$  and  $m_j$  for select measurement outcomes. First, Figure 4 displays  $V_{jk}$  for a uniform measurement outcome with  $|\tilde{s}\rangle = |\cdots \uparrow\uparrow\uparrow \cdots\rangle$ —which, along with its all-down partner, occurs with highest probability  $p_{\tilde{s}}^{(0)}$  (as confirmed numerically for systems as large as  $N = 26$ ). Panels (a) and (b) correspond to paramagnetic and critical ancilla, respectively. In the former,  $V_{jk}$  decays exponentially with  $|j-k|$ , while in the latter it decays as  $|j-k|^{-4}$ . In both cases  $m_j$  is translational invariant, as dictated by uniformity of the measurement outcome. Moreover, we have numerically verified that  $m_j$  saturates to a constant value with increasing system size in the paramagnetic case, whereas it slowly grows (at the level of the third decimal digit) for critical ancilla. The  $V_{jk}$  and  $m_j$  values discussed here can be combined to infer the (also uniform)  $m_j$  profile for case II, which at  $N \rightarrow \infty$  will simply differ from  $m_j$  for case I by a finite value given the ‘fast’ decay in  $V_{jk}$ .

The next-most-probable set of measurement outcomes correspond to configurations with isolated spin flips introduced into the uniform  $\tilde{s}$  string considered above. Rather than consider such outcomes, we next examine a lower-



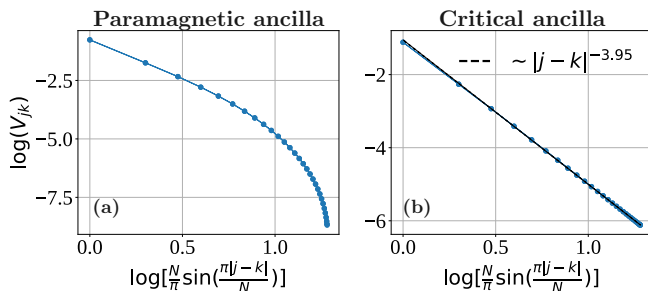


FIG. 4: (Color online).  $V_{jk}$  profiles for a uniform measurement outcome in case I of Table I. Translation invariance of the uniform string outcome implies that  $V_{jk}$  depends only on  $|j - k|$ . Decay in  $V_{jk}$  is exponential with paramagnetic ancilla (panel (a)) but power-law ( $\sim |j - k|^{-4}$ ) with critical ancilla (panel (b)). The data were obtained for  $N = 60$  using results from Appendix A.

probability configuration with two maximally separated domain walls:  $|\bar{s}\rangle = |\cdots \uparrow\uparrow\downarrow\downarrow\cdots\rangle$ . (Due to periodic boundary conditions considered here, domain walls come in pairs.) Figure 5 displays both  $V_{jk}$  and  $m_j$  for this measurement outcome assuming case I. Since  $V_{jk}$  now depends on  $j$  and  $k$  due to non-uniformity of the measurement outcome, in (a,b) we show  $V_{jk}$  versus  $k$  for three different  $j$  values. Decay with  $|j - k|$  similar to that for the uniform measurement outcome clearly persists here; see insets. In (c,d), the  $m_j$  profiles resemble those for the uniform case, but with dips near zero for  $j$ 's on either end of a given domain wall. We have also verified that still-lower-probability random  $\bar{s}$  strings also yield well-behaved  $V_{jk}$  and  $m_j$  couplings.

### B. $\tilde{X}$ measurement basis

Switching the ancilla measurement basis from  $\tilde{Z}$  to  $\tilde{X}$  qualitatively changes the statistical properties of  $m_j$  and  $V_{jk}$ . By construction, the initialized ancilla wavefunction  $|\psi_a\rangle$  is an eigenstate of the  $\mathbb{Z}_2$ -symmetry generator  $\tilde{G} = \prod_j \tilde{X}_j$  with eigenvalue  $+1$ . For  $\tilde{X}$ -basis measurements, a given ancilla state  $|\bar{s}\rangle$  obtained after a measurement can also be classified by its  $\tilde{G}$  eigenvalue; we refer to measurement outcomes with  $\tilde{G}|\bar{s}\rangle = +|\bar{s}\rangle$  as ‘even strings’ and outcomes with  $\tilde{G}|\bar{s}\rangle = -|\bar{s}\rangle$  as ‘odd strings’. (Due to the form of the unitary  $U$  applied prior to measurement in this case, both sectors can still arise despite the initialization.) Consider now an even-string measurement outcome with  $\langle \bar{s} | \psi_a \rangle \neq 0$ —as assumed in the perturbative expansion developed in Sec. III A. Crucially, due to mismatch in  $\tilde{G}$  eigenvalues,  $\langle \bar{s}(i_1 \cdots i_{N_f}) | \psi_a \rangle$  then vanishes for *any* odd number of flipped spins  $N_f$ . It follows that  $a(j) = 0$  in Eqs. (35) and (36), leaving

$$V_{jk} = a(j, k), \quad m_j = -2\theta + 2(\langle O \rangle - \theta) \sum_{k \neq j} V_{jk}. \quad (47)$$

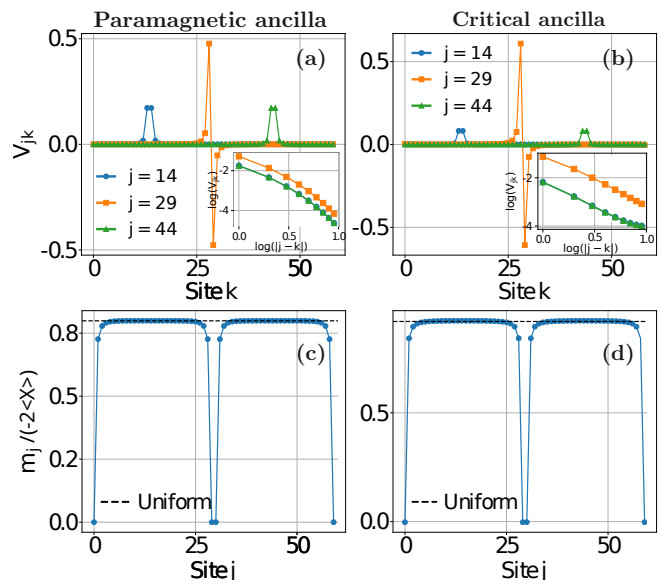


FIG. 5: (Color online).  $V_{jk}$  and  $m_j$  profiles for a two-domain-wall measurement outcome in case I of Table I. Domain walls reside near sites 0 and 30 in a system with  $N = 60$ . Left and right columns show data for paramagnetic and critical ancilla, respectively. Due to loss of translation symmetry, we show  $V_{jk}$  versus  $k$  for several  $j$  values. In all cases  $V_{jk}$  decays with  $|j - k|$ . The corresponding  $m_j$  profiles (panels (c,d)) exhibit dips near zero in the immediate vicinity of the domain walls, but are otherwise roughly uniform matching the values obtained for a uniform string outcome (black dashed lines). Data obtained using results from Appendix A.

Notice that  $V_{jk}$  here is always non-negative [recall the discussion below Eq. (41)].

The mean and variance of  $V_{jk}$  then reduce to simple ground-state ancilla correlation functions:

$$\bar{V}_{jk} = \langle \psi_a | \tilde{Z}_j \tilde{Z}_k | \psi_a \rangle, \quad \text{Var}(V_{jk}) = 1 - \langle \psi_a | \tilde{Z}_j \tilde{Z}_k | \psi_a \rangle^2. \quad (48)$$

At large  $|j - k|$ , the mean always decays to zero: for ancilla initialized in the paramagnetic phase with correlation length  $\xi$  we have  $\bar{V}_{jk} \sim e^{-|j-k|/\xi}$ , while if the ancilla are critical  $\bar{V}_{jk} \sim 1/|j - k|^{1/4}$ . The variance of  $V_{jk}$ , by contrast, grows towards unity at large  $|j - k|$ . Correspondingly, the  $V_{jk}$ 's for particular measurement outcomes can differ wildly from the mean, and in particular need not decay with  $|j - k|$ .

Remarkably, for case III in Table I  $m_j$  takes on the same  $j$ -independent value for *any* even-sector measurement outcome:

$$m_j^{\text{III}} = -2\langle X \rangle. \quad (49)$$

For case IV, however,  $m_j$  depends nontrivially on  $V_{jk}$  and

hence the measurement outcome; here we find

$$\bar{m}_j^{\text{IV}} = -2C \left( 1 + \sum_{k \neq j} \bar{V}_{jk} \right) \quad (50)$$

$$\text{Var}(m_j^{\text{IV}}) = (2C)^2 \sum_{k, k' \neq j} (\bar{V}_{kk'} - \bar{V}_{jk} \bar{V}_{jk'}) \quad (51)$$

with  $\bar{V}_{jk}$  given in Eq. (48). Suppose that the ancilla are paramagnetic. Exponential decay of  $\bar{V}_{jk}$  with  $|j - k|$  yields a finite mean  $\bar{m}_j^{\text{IV}}$ , though the variance diverges linearly with system size,  $\text{Var}(m_j^{\text{IV}}) \sim N$ , due to contributions from the  $\bar{V}_{kk'}$  term with  $k'$  near  $k$ . With critical ancilla, power-law decay of  $\bar{V}_{jk}$  generates divergent mean and variance:  $\bar{m}_j^{\text{IV}} \sim N^{3/4}$  and  $\text{Var}(m_j^{\text{IV}}) \sim N^{7/4}$ . In both scenarios the fluctuations of  $m_j$  increase with system size faster than the average value.

We therefore can only apply the perturbative formulation developed in Sec. III A to a restricted set of  $\tilde{X}$ -basis measurement outcomes that lead to a well-behaved, decaying interaction term in  $H_m$ , and correspondingly well-behaved  $m_j$  couplings. Fortunately, the most probable measurement outcomes do indeed satisfy these criteria.

Figure 6 plots  $V_{jk}$  for the highest-probability outcome, corresponding to the uniform string  $|\tilde{s}\rangle = |\cdots \rightarrow \rightarrow \rightarrow \cdots\rangle$  [66]. For (a) paramagnetic ancilla  $V_{jk}$  decays to zero with  $|j - k|$  exponentially, while for (b) critical ancilla it decays as  $\sim |j - k|^{-1}$ . In case IV with  $C \neq 0$ , Eq. (47) implies that the associated  $m_j$  converges to a finite value as  $N$  increases for paramagnetic ancilla, but diverges as  $\ln N$  with critical ancilla. (For  $C = 0$ ,  $m_j$  again simply vanishes.) Therefore, modulo this possible logarithmic factor, the uniform string presents a ‘good’  $\tilde{X}$ -basis measurement outcome.

As an example of a ‘bad’ measurement outcome, consider next the domain-wall configuration  $|\tilde{s}\rangle = |\cdots \rightarrow \rightarrow \rightarrow \leftarrow \leftarrow \leftarrow \cdots\rangle$ . Figure 7 shows that here  $V_{jk}$  becomes highly non-local. More precisely,  $V_{jk}$  takes on sizable values whenever both  $j$  and  $k$  reside in the ‘ $\leftarrow$ ’ domain, regardless of their separation. One can gain intuition for this observation by considering the ancilla ground state deep in the paramagnetic regime. Here the ground state takes the form  $|\psi_a\rangle = |\rightarrow \rightarrow \rightarrow \cdots \rightarrow\rangle + \cdots$ , where the ellipsis denotes perturbative corrections induced by small  $J_{\text{anc}}/h_{\text{anc}}$ . To leading order, these corrections involve spin flips on nearest-neighbor sites induced by  $J_{\text{anc}}$ , i.e., admixture of  $|\cdots \rightarrow \rightarrow \rightarrow \leftarrow \leftarrow \rightarrow \rightarrow \cdots\rangle$  components into the wavefunction. Now consider the domain-wall outcome  $|\tilde{s}\rangle$ . Flipping two spins at sites  $j, k$  in the energetically unfavorable  $\leftarrow$  domain tends to increase the overlap with the ground state—naturally leading to  $V_{jk} = \frac{\langle \tilde{s}(j,k) | \psi_a \rangle}{\langle \tilde{s} | \psi_a \rangle}$  that can exceed unity even for distant  $j, k$  as seen in our simulations. Flipping one spin within each of the two domains takes the energetically favorable ‘ $\rightarrow$ ’ domain and introduces a *single*  $\leftarrow$  spin. That domain then no longer resembles the ground state, which always harbors an even number of flipped spins. The coupling  $V_{jk}$  is therefore generically small with  $j$  and  $k$

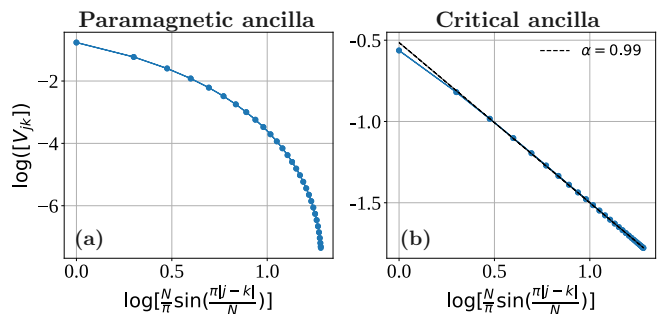


FIG. 6: (Color online).  $V_{jk}$  **profile for a uniform  $\tilde{X}$ -basis measurement outcome**. Decay of  $V_{jk}$  is exponential with paramagnetic ancilla and power-law ( $\sim |j - k|^{-1}$ ) with critical ancilla. In the critical case, note the significantly smaller exponent compared to Fig. 4. Data obtained using results from Appendix A with system size  $N = 60$ .

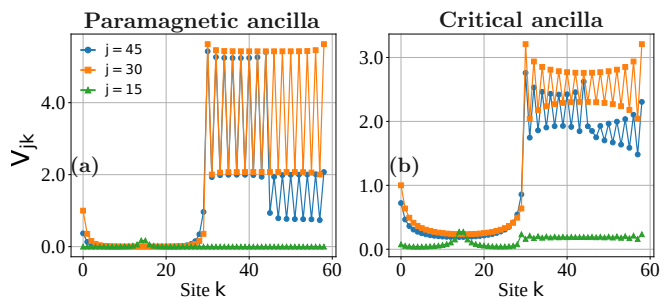


FIG. 7: (Color online).  $V_{jk}$  **profile for a two-domain-wall  $\tilde{X}$ -basis measurement outcome**. The first 30 sites point in the energetically favorable  $\rightarrow$  direction, while the remaining 30 sites point in the unfavorable  $\leftarrow$  direction. Non-decaying behavior of  $V_{jk}$  occurs when  $j, k$  both reside in the unfavorable domain. Data obtained using results from Appendix A for system size  $N = 60$ .

in opposite domains, also as borne out in our numerics. Finally, flipping two spins in the  $\rightarrow$  domain again decreases the resemblance with the ground state—more so as the separation between the flipped sites  $j$  and  $k$  increases. The corresponding  $V_{jk}$  diminishes with  $|j - k|$  in line with simulations yet again.

More generally, ‘good’ measurement outcomes are those for which flipping two far away spins invariably decreases overlap with the ground state such that  $V_{jk} \rightarrow 0$  as  $|j - k|$  increases. In addition to the highest-probability uniform string, the next-highest-probability set of strings—which contain dilute sets of nearest-neighbor flipped spins relative to the uniform background—also satisfy this property. Indeed, starting from such configurations, flipping spins at well-separated sites always locally produces regions with an odd number of flipped spins in a background of energetically favorable  $\rightarrow$  spins, thereby obliterating the overlap with the ancilla ground state and hence  $V_{jk}$ .

## V. PROTOCOL WITH $\tilde{Z}$ -BASIS MEASUREMENTS

We now use our perturbative formalism to examine how correlations in the critical chain are modified by particular outcomes of  $\tilde{Z}$ -basis ancilla measurements in our protocol. In Sec. IV we saw that for this measurement basis both the mean and variance of  $V_{jk}$  vanish as  $|j - k| \rightarrow \infty$ , suggesting that generic measurement outcomes yield well-behaved decaying interactions in  $H_m$  [Eq. (34)]. Moreover, with paramagnetic ancilla the variance of  $m_j$  trended to a finite value at large system sizes, suggesting that the single-body piece in  $H_m$  is also well-behaved for generic measurement outcomes. Thus for paramagnetic ancilla, below we proceed with confidence considering unrestricted measurement outcomes from the lens of the continuum defect-line action obtained in Sec. III B. For critical ancilla we saw that the variance of  $m_j$  grew slowly with system size, warranting more caution in this scenario.

Let us illustrate an example for case I where  $m_j \propto 1 - a(j)^2$  with  $a(j) = \frac{\langle \tilde{s}(j) | \psi_a \rangle}{\langle \tilde{s} | \psi_a \rangle}$ . After the uniform strings, the next most likely measurement outcomes are those containing a single spin flip. Consider one such state  $|\tilde{s}\rangle$  with a single flipped spin at site  $j_{\text{flip}}$ . Subsequently flipping the spin at  $j_{\text{flip}}$  converts  $|\tilde{s}\rangle$  back into the most probable, uniform string. We thereby obtain  $a(j_{\text{flip}}) > 1$  and hence  $m_{j_{\text{flip}}} < 0$  for this measurement outcome. With paramagnetic ancilla, this negative  $m_{j_{\text{flip}}}$  value saturates to a small constant as the system size increases. With critical ancilla, by contrast, we find that the magnitude of this negative value continues to increase over accessible system sizes—but *very* slowly similar to the standard deviation shown in the right panels of Figure 3. We thus expect our formalism to apply also to general  $\tilde{Z}$ -basis measurement outcomes even for critical ancilla, at least over system sizes relevant for experiments.

We now consider the unitaries in cases I and II from Table I in turn.

### A. Case I

We start with case I where the unitary reads  $U_j = e^{iu(X_j - \langle X \rangle)\tilde{X}_j}$ . This form of  $U_j$  preserves the  $Z_2$  symmetries  $G$  and  $\tilde{G}$  for the critical and ancilla chains, but does not preserve time reversal symmetry  $\mathcal{T}$  (which sends  $U_j \rightarrow U_j^\dagger$ ). Thus although the  $\tilde{Z}$ -basis measurements break  $\tilde{G}$  symmetry, the post-measurement state  $|\psi_{\tilde{s}}\rangle$  remains invariant under  $G$ . These considerations tell us that, for case I,  $U' = e^{iH'}$  in Eq. (22) is generically non-trivial [as one can indeed see from Eq. (33)] while  $H_m$  and hence  $\mathcal{S}_m$  must preserve  $G$  symmetry. Indeed, Eq. (34)

now takes the manifestly  $G$ -invariant form

$$H_m = u^2 \sum_j m_j (X_j - \langle X \rangle) + u^2 \sum_{j \neq k} V_{jk} (X_j - \langle X \rangle)(X_k - \langle X \rangle) \quad (52)$$

with

$$m_j = -2\langle X \rangle [1 - a(j)^2]. \quad (53)$$

and  $V_{jk}$  given (as for all cases) by Eq. (35). The defect-line action, using the low-energy expansion from Eq. (8), then reads

$$\mathcal{S}_m = u^2 \int_x m(x) \varepsilon(x, \tau = 0) + u^2 \int_{x,y} V(x, y) \varepsilon(x, \tau = 0) \varepsilon(y, \tau = 0). \quad (54)$$

Here  $m(x)$  and  $V(x, y)$  represent the coarse-grained, continuum-limit counterparts of  $m_j$  and  $V_{jk}$ .

Provided  $V(x, y)$  scales to zero faster than  $1/|x - y|$ —which is indeed generally the case both for paramagnetic and critical ancilla—we can approximate the second line of Eq. (54) as a local interaction obtained upon fusing the two  $\varepsilon$  fields according to the fusion rules summarized in Eq. (6). The leading nontrivial fusion product is  $-i\gamma_R \partial_x \gamma_R + i\gamma_L \partial_x \gamma_L$ , which is a descendent of the identity that, crucially, has a larger scaling dimension compared to the  $\varepsilon$  field appearing in the first line of Eq. (54) [49]. It follows that for capturing long-distance physics we can neglect the  $V(x, y)$  term altogether and simply take

$$\mathcal{S}_m \approx u^2 \int_x m(x) \varepsilon(x, \tau = 0). \quad (55)$$

We are primarily interested in computing the two-point correlator

$$\langle Z_j Z_{j'} \rangle_{\tilde{s}} \sim \langle \sigma(x_j) \sigma(x_{j'}) \rangle_{\tilde{s}} \quad (56)$$

in the presence of Eq. (55). Technically, according to Eq. (37) we need to conjugate the  $Z_j$  operators with the unitary  $U'$ , which in case I rotates  $Z$  about the  $X$  direction. Such a rotation only mixes in operators in the low-energy theory with (much) larger scaling dimension compared to  $\sigma$  [67]. Hence Eq. (56)—which is the same as what one would obtain by ignoring  $U'$  altogether—continues to provide the leading decomposition for the correlator.

When  $m(x)$  is independent of  $x$ , as arises for uniform measurement outcomes, the above defect line action is marginal, though for general measurement outcomes  $m(x)$  retains nontrivial  $x$  dependence. References 55–57 employed non-perturbative field-theory methods to study the effects of this type of defect line on spin-spin correlation functions in the two dimensional Ising model. In

particular, Ref. 57 derived the spin-spin correlation function for an  $\varepsilon$  line defect whose coupling is an arbitrary function of position. We report here their main result:

$$\langle \sigma(x)\sigma(x') \rangle_{\tilde{s}} \sim |x - x'|^{-\frac{1}{4} - \frac{\kappa u^2}{8}} [m(x) + m(x')] e^{\frac{\kappa u^2}{16} F(x, x')}, \quad (57)$$

where

$$\begin{aligned} F(x, x') &= \int_x^{x'} dy m(y) \frac{d}{dy} \ln \left[ \frac{[(y - x')^2 + a^2]^{1 + \kappa u^2 m(x')}}{[(y - x)^2 + a^2]^{1 + \kappa u^2 m(x)}} \right. \\ &\quad \left. - \int_x^{x'} dy dy' [1 + \kappa u^2 m(y')] \left[ \frac{d}{dy} m(y) \right] \right. \\ &\quad \left. \times \frac{d}{dy'} \ln[(y - y')^2 + a^2] \right]. \end{aligned} \quad (58)$$

Above,  $a$  is a short-distance cutoff, and  $\kappa$  is a dimensionless parameter that captures an overall constant neglected on the right side of Eq. (8) as well as difference in normalization conventions between our work and Ref. 57. We simply view  $\kappa$  as a fitting parameter in our analysis. Since  $F(x, x')$  in Eq. (57) already contains an  $O(u^2)$  prefactor, to the order we are working it suffices to simply set  $u = 0$  in Eq. (58). Some algebra then gives the far simpler expression

$$\langle \sigma(x)\sigma(x') \rangle_{\tilde{s}} \sim |x - x'|^{-\frac{1}{4} - \frac{\kappa u^2}{4}} [m(x) + m(x')] e^{\frac{\kappa u^2}{8} f(x, x')} \quad (59)$$

with

$$f(x, x') = \int_x^{x'} dy \ln \left[ \frac{(y - x)^2 + a^2}{(y - x')^2 + a^2} \right] \frac{d}{dy} m(y). \quad (60)$$

Eqs. (59) and (60) capture coarse-grained spin-spin correlations for general measurement outcomes, though for deeper insight we now explicitly examine some special cases.

For a uniform measurement outcome (e.g.,  $s_j = +1$  for all  $j$ ) giving constant  $m(x) \equiv m_{\text{const}}$ , Eq. (59) simplifies to

$$\langle \sigma(x)\sigma(x') \rangle_{\tilde{s}} \sim \frac{1}{|x - x'|^{2\Delta_\sigma(u)}}, \quad (\text{uniform } \tilde{s}) \quad (61)$$

$$\Delta_\sigma(u) = \frac{1}{8}(1 + 2\kappa u^2 m_{\text{const}}), \quad (62)$$

consistent with the result found in Refs. 55 and 56 in the limit  $|x - x'| \gg a$  and to  $O(u^2)$ . Remarkably, the defect line in this post-selection sector yields an  $O(u^2)$  change in the scaling dimension of the  $\sigma$  field compared to the canonical result in Eq. (5). We confirm this change using infinite DMRG simulation reported in Figure 8: with both paramagnetic and critical ancilla, the scaling dimension of the  $\sigma$  field,  $\Delta_\sigma(u)$ , exceeds  $1/8$  when  $u \neq 0$ . The enhancement is quite similar for the paramagnetic and critical cases, as expected given that  $m_j$  is only slightly larger in the latter [see Figure 5(c, d)]. Figure 9 shows the

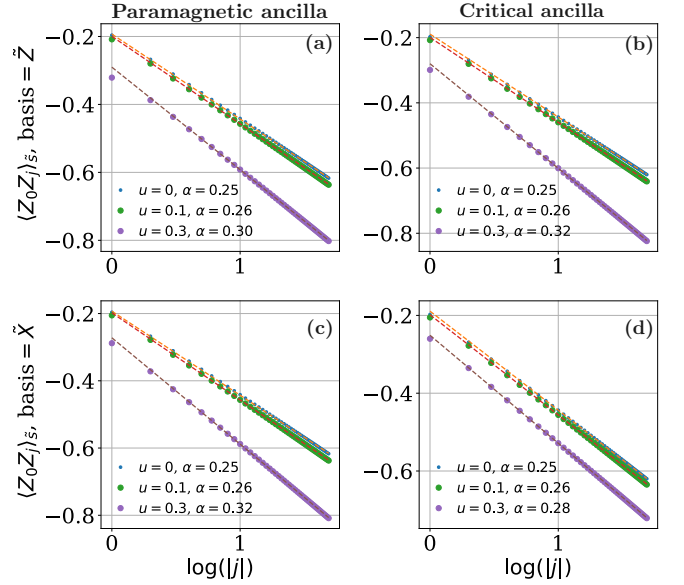


FIG. 8: (Color online). **Correlation function**  $\langle Z_0 Z_j \rangle_{\tilde{s}}$  **for uniform measurement outcomes**. The first row corresponds to case I from Table I while the second row corresponds to case III. At  $u = 0$  the curves exhibit an exponent  $1/4$  that follows from the pristine Ising CFT. Turning on  $u \neq 0$  yields a measurement-induced *increase* in the scaling dimension in all panels—as predicted by Eq. (62) for case I and (76) for case III. Data were obtained using infinite DMRG with bond dimension 1000 for paramagnetic ancilla and 2000 for critical.

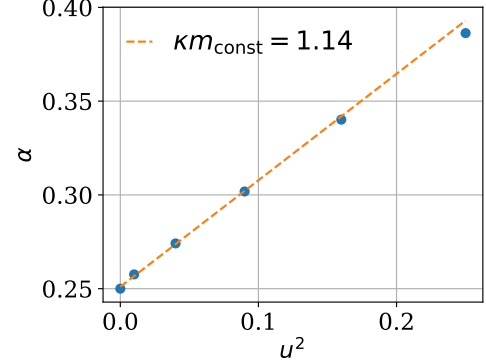


FIG. 9: (Color online). **Scaling of the power-law exponent for  $\langle Z_0 Z_j \rangle_{\tilde{s}}$  with a uniform measurement outcome**. Data correspond to case I in Table I assuming paramagnetic ancilla, and were obtained using iDMRG. The numerically extracted exponent  $\alpha$  scales approximately linearly with  $u^2$  at small  $u$ , in quantitative agreement with  $2\Delta_\sigma(u)$  predicted by Eq. (62). A linear fit to Eq. (62) yields  $\kappa m_{\text{const}} = 1.14$ .

dependence of the numerically extracted power-law exponent  $\alpha$  as a function of  $u^2$ , revealing a linear dependence in agreement with Eq. (62). The linear fit also allows us to extract a value  $\kappa = -1.12$ ; note that  $\kappa m_{\text{const}} > 0$ —ensuring that  $\Delta_\sigma(u)$  increases with  $u$  in the presence of the defect line as observed in our numerical simulations.

Next we examine a measurement outcome  $|\bar{s}\rangle = |\cdots \uparrow\uparrow\uparrow\downarrow\downarrow\downarrow \cdots\rangle$  with a domain wall. This outcome yields nearly uniform  $m_j$ —see black dashed lines in Figs. 5(c,d)—except for a window around the domain wall where it approximately vanishes. We model the associated continuum  $m(x)$  profile as

$$m(x) = m_{\text{const}} \{ \Theta[(x_0 - d) - x] + \Theta[x - (x_0 + d)] \}, \quad (63)$$

where  $x_0$  is the domain-wall location,  $d$  is the spatial extent of suppressed  $m(x)$  region on either side and  $\Theta$  is the Heaviside function. Adequately capturing detailed behavior near the domain wall likely requires incorporating short-distance physics, though we expect that our low-energy framework can describe correlations among operators sufficiently far from  $x_0$ . With this restriction in mind, we consider the two-point correlator  $\langle \sigma(x)\sigma(x') \rangle_{\bar{s}}$  with  $x$  far to the left of the domain wall ( $x \ll x_0$ ) and  $x' > x$ . If  $x'$  also sits to the left of the domain wall, then  $f(x, x') = 0$  and the correlator retains—within our approximation—exactly the same form as in Eq. (61). If, however,  $x'$  sits to the right of the domain wall with  $x' \gg x_0$ , then we obtain

$$f(x, x') \approx 4dm_{\text{const}} \left( \frac{1}{x_0 - x} + \frac{1}{x' - x_0} \right), \quad (64)$$

resulting in a modest enhancement of the correlator amplitude compared to the domain-wall-free case. Summarizing, for the single-domain-wall measurement outcome we get

$$\langle \sigma(x)\sigma(x') \rangle_{\bar{s}} \sim \begin{cases} \frac{1}{|x-x'|^{2\Delta_\sigma(u)}}, & x' \ll x_0 \\ \frac{e^{\frac{1}{2}\kappa u^2 dm_{\text{const}} \left( \frac{1}{x_0-x} + \frac{1}{x'-x_0} \right)}}{|x-x'|^{2\Delta_\sigma(u)}}, & x' \gg x_0 \end{cases}. \quad (65)$$

To test Eq. (65), we performed DMRG simulations for a system of size  $N = 256$  system with open boundary conditions, so that we can accommodate a single-domain-wall measurement outcome. Figure 10 plots the numerically determined function

$$\delta \langle Z_j Z_{j'} \rangle \equiv \frac{\langle Z_j Z_{j'} \rangle_{\bar{s}, \text{DW}} - \langle Z_j Z_{j'} \rangle_{\bar{s}, \text{unif}}}{\langle Z_j Z_{j'} \rangle_{\bar{s}, \text{unif}}}, \quad (66)$$

i.e., the difference in the microscopic two-point correlator with and without a domain wall, normalized by the correlator for the uniform measurement outcome. Quite remarkably, the figure reveals the main qualitative features predicted by our result in Eq. (65): When both  $j$  and  $j'$  sit to the left of the domain wall, the difference in correlators approaches zero, while the correlator in the presence of a domain wall exhibits a small enhancement when  $j$  and  $j'$  sit on opposite sides of the domain wall. Moreover, the enhancement factor modestly increases as  $j$  approaches the domain wall—also in harmony with Eq. (65). The agreement between numerics and analytics here provides a very nontrivial check on our formalism.

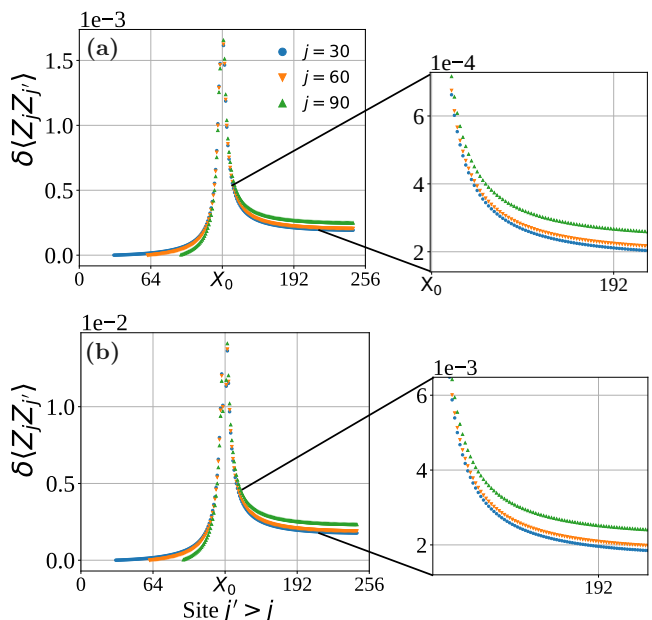


FIG. 10: (Color online). **Relative correlation function**  $\delta \langle Z_j Z_{j'} \rangle$  [Eq. (66)] for a domain-wall measurement outcome in case I from Table I. Main panels illustrate the relative change in the two-point function resulting from insertion of a domain wall. Panel (a) corresponds to  $u = 0.1$ , and panel (b) to  $u = 0.3$ . The domain wall resides near site  $x_0 = 128$  in an  $N = 256$  system with open boundary conditions. When  $j$  and  $j'$  both sit on one side of the domain wall, the change in correlations is negligible. When they sit on opposite sides, however, the correlations *increase* relative to the uniform measurement outcome. As discussed in the main text, the behavior captured here reproduces the main qualitative features of the analytical prediction in Eq. (65). Data were obtained using DMRG with paramagnetic ancilla.

In the presence of multiple well-separated dilute domain walls, the behavior of the correlator  $\langle \sigma(x)\sigma(x') \rangle_{\bar{s}}$  follows from a straightforward generalization of Eq. (65). For  $x$  and  $x'$  within the same domain, the correlator again reproduces that in a uniform measurement outcome, whereas moving  $x'$  rightward leads to a relative uptick in the correlator upon passing successive domain walls. For dense domain walls, the  $m_j$  pattern changes significantly, necessitating a separate analysis.

## B. Case II

The unitary in case II,  $U_j = e^{iu(Z_j - C)\tilde{X}_j}$ , is invariant under  $\tilde{G}$  but preserves neither  $G$  nor  $\mathcal{T}$ . Thus the post-measurement state generically breaks all microscopic symmetries. A special case arises, however, when  $C = 0$ : here  $U_j$  and hence the post-measurement state preserve the composite operation  $G\mathcal{T}$ . In line with these

symmetry considerations, case II yields

$$H_m = u^2 \sum_j m_j Z_j + u^2 \sum_{j \neq k} V_{jk} Z_j Z_k \quad (67)$$

with

$$m_j = -2C \left[ 1 - a(j)^2 + \sum_{k \neq j} V_{jk} \right]. \quad (68)$$

Indeed, the  $m_j$  term—which is odd under  $G$ —appears as long as  $C \neq 0$ . The unitary  $U' = e^{iH'}$ , by contrast, is generically nontrivial even for  $C = 0$  and always preserves  $GT$ :  $H'$  in Eq. (33) is odd under  $G$  in case II, but in  $U'$  the minus sign is undone by  $i \rightarrow -i$  from time reversal. Nevertheless, we only consider  $Z_j$  correlators below, which here are invariant under conjugation by  $U'$ .

The associated continuum defect-line action, now using Eq. (7), is

$$\begin{aligned} \mathcal{S}_m = & u^2 \int_x m(x) \sigma(x, \tau = 0) \\ & + u^2 \int_{x,y} V(x,y) \sigma(x, \tau = 0) \sigma(y, \tau = 0). \end{aligned} \quad (69)$$

As in case I,  $V(x,y)$  decays fast enough that we can approximate the second line with a local interaction, obtained here by fusing the pair of  $\sigma$  fields. The leading nontrivial fusion product is  $\varepsilon$  [see Eq. (6)]. For  $C = 0$ , where the  $m(x)$  term drops out by symmetry, Eq. (69) then reduces to the form

$$\mathcal{S}_m = u^2 \int_x M(x) \varepsilon(x, \tau = 0), \quad (C = 0) \quad (70)$$

studied in the previous subsection with  $M(x) = \int_y V(x,y)$ . One-point correlators  $\langle Z_j \rangle_{\tilde{s}}$  vanish by symmetry while two-point correlators  $\langle Z_j Z_{j'} \rangle_{\tilde{s}}$  can be computed using the methods deployed above. For the remainder of this subsection we therefore take  $C \neq 0$ . In this regime the  $\sigma$  field arising from first line of Eq. (69) has a smaller scaling dimension compared to the  $\varepsilon$  field emerging from the second line. We can therefore neglect the latter term, yielding

$$\mathcal{S}_m \approx u^2 \int_x m(x) \sigma(x, \tau = 0), \quad (C \neq 0). \quad (71)$$

Physically,  $m(x)$  plays the role of a longitudinal magnetic field that acts only at  $\tau = 0$ .

For uniform strings where  $m(x) = m_{\text{const}}$ , the defect-line action in Eq. (71) constitutes a strongly relevant perturbation. Clearly then  $\sigma(x, \tau = 0)$  and hence  $Z_j$  take on uniform, non-zero expectation values in this post-selection sector:

$$\langle Z_j \rangle_{\tilde{s}} \sim \langle \sigma(x_j) \rangle_{\tilde{s}} = g(u), \quad (\text{uniform } \tilde{s}), \quad (72)$$

where the function  $g(u)$  vanishes with  $u$  but tends to a non-zero constant at  $u \neq 0$  in the thermodynamic limit.

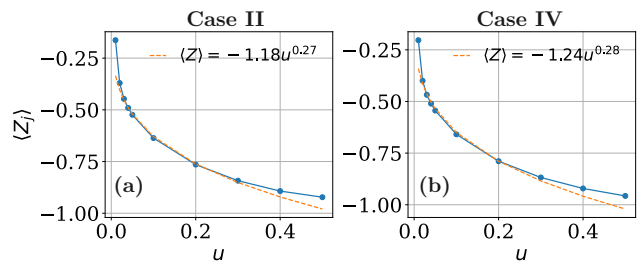


FIG. 11: (Color online). **One-point function  $\langle Z_j \rangle$  with a uniform measurement outcome.** Panels (a) and (b) respectively correspond to cases II and IV from Table I. Results were obtained using infinite DMRG with  $C = -1$ , assuming paramagnetic ancilla. The non-zero value generated by measurement at  $u \neq 0$  validates analytic predictions, e.g., Eq. (72). Moreover, the fits shown by the dashed lines exhibit excellent agreement with the  $u$  dependence extracted using renormalization group arguments.

Infinite DMRG results for  $\langle Z_j \rangle_{\tilde{s}}$ , presented in Figure 11 confirm this behavior.

We apply the renormalization group (RG) technique to obtain the dependence of  $\langle \sigma(x_j) \rangle_{\tilde{s}}$  on  $u$ . Rescaling the spatial coordinate  $x$  by a factor  $b$  and defining  $x' = x/b$ , the  $\sigma$  field transforms as  $\sigma(x) = b^{-1/8} \sigma'(x')$ . The defect-line action  $\mathcal{S}_m = u^2 m_{\text{const}} \int dx \sigma(x)$  is then rewritten as  $\mathcal{S}_m = u^2 m_{\text{const}} b^{1-1/8} \int dx' \sigma'(x')$  and in particular exhibits a renormalized coupling strength  $u^2 b^{7/8}$ . Suppose now that at some coupling strength  $u_{\text{ref}}^2$ , the magnetization is a fixed constant  $\langle \sigma'(0) \rangle_{\tilde{s}} = M_{\text{ref}}$ . We can back out the observables at arbitrary  $u$  by finding the RG map that takes  $u \rightarrow u_{\text{ref}}$ . First, choose the scaling parameter  $b$  such that  $u^2 b^{7/8} = u_{\text{ref}}^2$ , i.e.,  $b = (u/u_{\text{ref}})^{-16/7}$ . We then obtain  $\langle \sigma(0) \rangle_{\tilde{s}} = b^{-1/8} M_{\text{ref}} \propto u^{2/7}$ . Despite the simplicity of this argument, a fit of  $\langle Z_j \rangle$  in Figure 11 yields a scaling  $\sim u^{0.27}$  with an exponent that agrees well with our prediction of  $2/7 \approx 0.29$ .

We are not aware of works that compute the one-point function in the presence of arbitrary position-dependent  $m(x)$ 's that arise with generic measurement outcomes. Nevertheless, we expect that, at least for smoothly varying  $m(x)$  profiles,  $\langle \sigma(x) \rangle_{\tilde{s}}$  polarizes for each  $x$  with an orientation determined by the sign of  $m(x)$ . Since  $m_j$  averages to zero as shown in Sec. IV, averaging  $\langle Z_j \rangle_{\tilde{s}}$  over measurement outcomes then naturally erases the effects of measurements as must be the case on general grounds. In contrast, such cancellation need not arise when averaging  $\langle Z_j \rangle_{\tilde{s}}^2$  over measurement outcomes. We thus anticipate that

$$\sum_{\tilde{s}} p_{\tilde{s}} \langle Z_j \rangle_{\tilde{s}}^2 \neq 0. \quad (73)$$

Very crudely, if for a random measurement outcome  $\langle Z_j \rangle_{\tilde{s}} \sim u^2 m_j$ , then the nonlinear average above would be proportional to  $u^4 \text{Var}(m_j)$ . Our exact diagonalization results presented in Figure 12 support these predictions. The top panels show  $\langle Z_j \rangle_{\tilde{s}}^2$  averaged over all  $Z$ -basis mea-

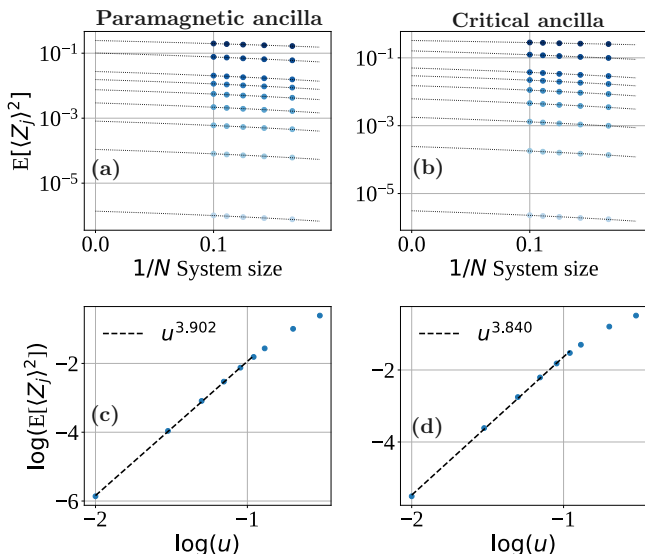


FIG. 12: (Color online). **Average of  $\langle Z_i \rangle_{\tilde{s}}$  over measurement outcomes in case II of Table I.** Data were obtained using exact diagonalization for two chains of length  $N = 6, 7, 8, 9, 10$  with  $C = -1$ . Panels (a, b) reveal well-behaved scaling with system size; larger values of  $u$  correspond to darker blue, with the darkest color corresponding to  $u = 0.13$ . Panels (c, d) show the extrapolated dependence of  $E(\langle Z_j \rangle_{\tilde{s}}^2)$  with  $u$ . For small  $u$ , we find  $\sim u^4$  scaling, consistent with the crude expectation that  $\langle Z_j \rangle_{\tilde{s}} \sim u^2 m_j$  for a particular measurement outcome.

surement outcomes versus  $1/N$  for several values of  $u$ . For both paramagnetic and critical ancilla, extrapolation to  $N \rightarrow \infty$  yields nonzero values for all  $u \neq 0$  cases; additionally, the lower panels show that the extrapolated values indeed scale very nearly as  $u^4$  for small  $u$  in both cases.

## VI. PROTOCOL WITH $\tilde{X}$ -BASIS MEASUREMENTS

Recall that for  $\tilde{X}$ -basis measurements, our perturbative formalism applies only to the highest probability subset of even-string ( $\tilde{G} |\tilde{s}\rangle = +|\tilde{s}\rangle$ ) measurement outcomes. These outcomes, to which we exclusively focus in this section, include the uniform state with  $\tilde{s}_j = +1$  on every site, and descendant states containing a dilute set of adjacent spin flips. Interestingly, even in this restricted space of measurement outcomes, we will encounter qualitative differences between paramagnetic versus critical ancilla in our protocol.

For both cases III and IV, the unitary  $U' = e^{iH'}$  is trivial in the even-string measurement sector. This result immediately follows from Eq. (33) using the fact that  $a(j) = 0$  for any even-string  $\tilde{s}$ . Hence in the ensuing analysis we need only consider  $H_m$  and the associated defect-line action  $\mathcal{S}_m$ . Note also that the  $U_j$  unitaries for cases III and IV explicitly violate  $\tilde{G}$  sym-

metry; nevertheless, ancilla measurements project onto an even-string  $\tilde{s}$  (by assumption), so that both the initial and post-measurement states are  $\tilde{G}$  eigenstates with eigenvalue  $+1$ . The situation is reversed compared to the protocol with  $\tilde{Z}$ -basis measurements, where the  $U_j$  unitaries preserved  $\tilde{G}$  while measurements produced a wavefunction that was not a  $\tilde{G}$  eigenstate.

### A. Case III

The case-III unitary  $U_j = e^{iu(X_j - \langle X \rangle) \tilde{Z}_j}$  yields a defect-line action

$$\mathcal{S}_m = u^2 m \int_x \varepsilon(x, \tau = 0) + u^2 \int_{x,y} V(x, y) \varepsilon(x, \tau = 0) \varepsilon(y, \tau = 0). \quad (74)$$

Equation (74) has the same form as Eq. (54) from case I—with the crucial difference that here  $m(x)$  is replaced with a constant  $m = -2\langle X \rangle$  that is the same for all of the (restricted) strings that we consider. For paramagnetic ancilla, results from Sec. IV imply that  $V(x, y)$  decays exponentially with  $|x - y|$ , allowing us to once again fuse the  $\varepsilon$ 's in the second line into a subleading term compared to the first. More care is needed for critical ancilla, since for the uniform string outcome  $V(x, y)$  decays like  $1/|x - y|$ . The second line then represents an inherently long-range, power-law-decaying interaction. Such a term is, however, still less relevant by power-counting compared to the first line. Thus, similar to case I, we can approximate the defect-line action as simply

$$\mathcal{S}_m \approx u^2 m \int_x \varepsilon(x, \tau = 0). \quad (75)$$

Spin-spin correlators correspondingly behave as

$$\langle \sigma(x) \sigma(x') \rangle_{\tilde{s}} \sim \frac{1}{|x - x'|^{2\Delta_\sigma(u)}}, \quad \Delta_\sigma(u) = \frac{1}{8}(1 + 2\kappa u^2 m). \quad (76)$$

At least within the approximations used here, a pristine power-law with  $O(u^2)$  enhanced scaling dimension occurs for any even-string measurement outcome conforming to our perturbative formalism, even if the outcome is not translationally invariant. Surely additional ingredients beyond those considered here would restore dependence on the measurement outcome; such terms, however, reflect subleading contributions, e.g., the neglected  $V(x, y)$  term above. By contrast, for case I the dependence on measurement outcome was already encoded in the leading  $m(x)\varepsilon$  term in the defect-line action.

The lower panels of Figure 8 confirm the modified power-law behavior for the uniform measurement outcome. Notice that for  $u = 0.1$ , the fitted scaling dimension is nearly the same for cases I and III, and for both paramagnetic and critical ancilla. This similarity is expected from our perturbative framework given that the

leading defect-line actions [Eqs. (55) and (75)] take the same form with similar coupling strengths in the uniform measurement outcome sector. At the larger value of  $u = 0.3$ , the extracted scaling dimensions in case III differ for paramagnetic and critical ancilla—even though our  $O(u^2)$  theory predicts precisely the same exponent in both scenarios. Such a correction is not surprising, given that at higher orders in  $u$ , even the leading term in the defect-line action can discriminate between paramagnetic and critical ancilla. Indeed, we have checked that in the paramagnetic case  $\Delta_\sigma(u)$  scales like  $u^2$  over a wider range of  $u$  compared to the case with critical ancilla.

### B. Case IV

For case IV, with unitary  $U_j = e^{iu(Z-C)\tilde{Z}}$ , the defect-line action reads

$$\begin{aligned} \mathcal{S}_m = & u^2 \int_x m(x) \sigma(x, \tau = 0) \\ & + u^2 \int_{x,y} V(x,y) \sigma(x, \tau = 0) \sigma(y, \tau = 0), \end{aligned} \quad (77)$$

which has identical structure to that of case II but with modified couplings  $m(x)$  and  $V(x,y)$  due to the shift in ancilla measurement basis. As in case II, the special limit  $C = 0$  still yields  $m(x) = 0$ , as required by symmetry.

Let us first take  $C \neq 0$ . Following the logic used for case III above, the second line is always subleading compared to the first, independent of whether the ancilla are paramagnetic or critical. For the uniform or nearly uniform measurement outcomes that we can treat here, the strongly relevant  $m(x)\sigma$  perturbation leads once again to a non-zero one-point function  $\langle \sigma \rangle_{\bar{s}} \neq 0$ , as reproduced in DMRG simulations [Figure 11(b)]. Similar to our previous discussion in case II, we numerically find that  $\langle Z_j \rangle_{\bar{s}}^2$  averaged over all measurement outcomes also appears to yield a non-zero value at large  $N$  (at least for paramagnetic ancilla), even though our perturbative formulation now only applies to a restricted set of measurement outcomes. See Figure 13 and notice the rather different scaling with  $u$  compared to Figure 12. The results for critical ancilla, however, did not show an obvious trend and so we do not report them.

When  $C = 0$ , the approximation invoked above no longer applies, and the defect-line action instead becomes

$$\mathcal{S}_m = u^2 \int_{x,y} V(x,y) \sigma(x, \tau = 0) \sigma(y, \tau = 0), \quad (C = 0). \quad (78)$$

Here the nature of the initial ancilla state becomes pivotal. For gapped ancilla, exponential decay in  $V(x,y)$  enables fusing the  $\sigma$  fields into a single  $\varepsilon$  field. One then obtains the form in Eq. (70) that, for uniform or nearly uniform measurement outcomes, modifies the power-law correlations in  $\langle \sigma(x)\sigma(x') \rangle_{\bar{s}}$  as described previously. For critical ancilla this prescription breaks down since  $V(x,y)$

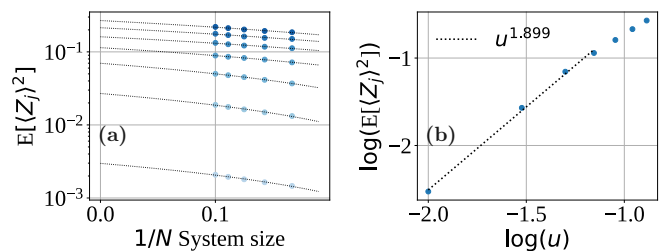


FIG. 13: (Color online). **Average of  $\langle Z_i \rangle_{\bar{s}}^2$  over measurement outcomes in case IV of Table I.** All parameters are the same as in Fig. 12, except here we consider only paramagnetic ancilla. The scaling of  $E(\langle Z_j \rangle_{\bar{s}}^2)$  with  $u$  in panel (b) is much steeper ( $\sim u^2$ ) compared to the scaling found in Fig. 12.

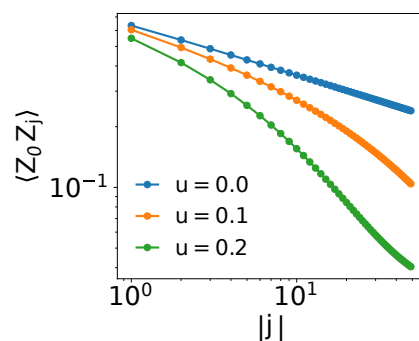


FIG. 14: (Color online). **Correlation function  $\langle Z_0 Z_j \rangle_{\bar{s}}$  for case IV in Table I with  $C = 0$  and critical ancilla.** At  $u > 0$  the correlator appears to decay faster than a power-law over the  $j$  range shown, as anticipated from the measurement-induced long-range interaction in Eq. (78). Data were obtained using iDMRG with bond dimension 2000.

scales like  $1/|x - y|$ . The resulting power-law-decaying interaction between  $\sigma$ 's in Eq. (78) is strongly relevant by power counting; the system's fate then depends on whether the power-law interaction is ferromagnetic or antiferromagnetic. On one hand, ferromagnetic  $\sigma(x, \tau = 0)\sigma(y, \tau = 0)$  interaction would promote order-parameter correlations—possibly replacing power-law decay in the spin-spin correlation function with true long-range order, i.e., turning the critical chain into a cat state. On the other, antiferromagnetic interaction would suppress order parameter correlations, potentially yielding an exponentially decaying correlator. Since  $V(x,y)$  is always non-negative in case IV,  $\mathcal{S}_m$  in Eq. (78) realizes the antiferromagnetic scenario. Our DMRG simulations presented in Figure 14 recover fast-than-power-law suppression induced by measurements, in at least qualitative agreement with the above expectations. We are unable to resolve, however, whether the correlations decay exponentially.



## VII. EXACT AVERAGING OVER EVEN/ODD STRINGS IN $\tilde{X}$ -MEASUREMENT PROTOCOL

With  $\tilde{X}$ -basis measurements, outcomes  $\tilde{s}$  can be divided into sectors according to whether  $\tilde{G}|\tilde{s}\rangle = +|\tilde{s}\rangle$  or  $-|\tilde{s}\rangle$ . Here we exploit this neat even/odd-string dichotomy to obtain illuminating, exact expressions for the average of critical-chain observables  $A$  over measurement outcomes confined to a particular  $\epsilon = \pm 1$  parity sector. Using Eqs. (18) and (19), the average in sector  $\epsilon$  reads

$$\begin{aligned} \langle A \rangle_\epsilon &= \sum_{\tilde{s} \in \epsilon} p_{\tilde{s}} \langle \psi_{\tilde{s}} | A | \psi_{\tilde{s}} \rangle \\ &= \sum_{\tilde{s} \in \epsilon} \langle \psi_a | \langle \psi_c | U^\dagger \left( \prod_j |\tilde{s}_j\rangle \langle \tilde{s}_j| \right) U A_U | \psi_c \rangle | \psi_a \rangle \\ &= \langle \psi_a | \langle \psi_c | U^\dagger \tilde{P}_\epsilon U A_U | \psi_c \rangle | \psi_a \rangle, \end{aligned} \quad (79)$$

where  $U = \prod_j U_j$  represents the unitary applied prior to measurement and  $A_U = U^\dagger A U$ . In the last line

$$\tilde{P}_\epsilon = \sum_{\tilde{s} \in \epsilon} |\tilde{s}\rangle \langle \tilde{s}| = \frac{1}{2} (1 + \epsilon \tilde{G}) \quad (80)$$

projects onto the measurement-outcome sector with parity  $\epsilon$ . For the unitaries in either case III or IV from Table I, the anticommutation relation  $\{\tilde{Z}_j, \tilde{G}\} = 0$  implies that  $U^\dagger \tilde{G} = \tilde{G} U$ . We can therefore express Eq. (79), after also using  $\tilde{G}|\psi_a\rangle = |\psi_a\rangle$ , as

$$\begin{aligned} \langle A \rangle_\epsilon &= \frac{1}{2} \langle \psi_a | \langle \psi_c | A_U | \psi_c \rangle | \psi_a \rangle \\ &\quad + \frac{\epsilon}{2} \langle \psi_a | \langle \psi_c | U^2 A_U | \psi_c \rangle | \psi_a \rangle. \end{aligned} \quad (81)$$

Notice that the second term is real for any Hermitian operator  $A$ , since any imaginary parts vanish by parity constraints. Summing over the even and odd sectors yields  $\langle A \rangle_+ + \langle A \rangle_- = \langle \psi_a | \langle \psi_c | A_U | \psi_c \rangle | \psi_a \rangle$ —which, in agreement with Eq. (20), is simply the result one would obtain without performing any measurements. The difference between the even- and odd-sector correlators, by contrast, isolates the second term in Eq. (81),

$$\langle A \rangle_+ - \langle A \rangle_- = \langle \psi_c | \langle \psi_a | U^2 A_U | \psi_c \rangle | \psi_a \rangle, \quad (82)$$

and *does* retain nontrivial imprints of the measurements enacted in our protocol. Equation (82) is equivalent to the expectation value of the *non-local* operator  $A\tilde{G}$  taken in the pre-measurement state  $U|\psi_c\rangle|\psi_a\rangle$ ; crucially, measuring the ancilla in the  $\tilde{X}$  basis provides access to such non-local information.

There is, however, no free lunch here: On general grounds the right side of Eq. (82) should decay to zero with system size  $N$  for any fixed  $u \neq 0$ . To see why, let  $p_\epsilon = \sum_{\tilde{s} \in \epsilon} p_{\tilde{s}}$  denote the probability for obtaining parity sector  $\epsilon$  after a measurement, and consider the difference

$$p_+ - p_- = \langle \psi_c | \langle \psi_a | U^2 | \psi_c \rangle | \psi_a \rangle. \quad (83)$$

Equation (83) simply corresponds to Eq. (82) with  $A$  being the identity. At  $u = 0$ , where  $U$  also reduces to the identity, we obtain  $p_+ - p_- = 1$ —reflecting the fact that the initial ancilla state  $|\psi_a\rangle$  resides in the even-parity sector by construction. Turning on  $u \ll 1$ , the state  $U^2|\psi_c\rangle|\psi_a\rangle = \prod_j U_j^2|\psi_c\rangle|\psi_a\rangle$  exhibits a small  $O(u^2)$  probability for flipping a particular  $\tilde{X}$ -basis ancilla spin. Yet the net effect over a macroscopic number of sites  $N$  inevitably translates into a ‘large’ change in the probability for remaining in the even-parity sector. In terms of Eq. (83), this logic implies that  $U^2|\psi_c\rangle|\psi_a\rangle$  becomes orthogonal to  $|\psi_c\rangle|\psi_a\rangle$  at fixed  $u \neq 0$  with  $N \rightarrow \infty$ , leading to  $p_+ - p_- \approx 0$ . The insertion of  $A_U$  in Eq. (82), assuming it represents physically relevant combinations of local operators, can not change this conclusion, implying that  $\langle A \rangle_+ - \langle A \rangle_-$  vanishes with  $N$  as well.

We propose the ratio

$$r(A) \equiv \frac{\langle A \rangle_+ - \langle A \rangle_-}{p_+ - p_-} = \frac{\langle \psi_c | \langle \psi_a | U^2 A_U | \psi_c \rangle | \psi_a \rangle}{\langle \psi_c | \langle \psi_a | U^2 | \psi_c \rangle | \psi_a \rangle} \quad (84)$$

as an appealing diagnostic of  $\tilde{X}$ -basis measurement effects on Ising criticality. Equation (84) needs not vanish in the thermodynamic limit. Moreover, both the numerator and denominator comprise linear averages over experimentally accessible quantities, circumventing the need for post-selection. (But again there is no free lunch—the individually small numerator and denominator would need to be obtained with sufficient accuracy to yield a meaningful ratio.)

Inspired by our perturbative results for a restricted set of even-sector measurement outcomes, we conjecture that for case III

$$r(Z_j Z_k) \sim |j - k|^{-2\Delta(u)} \quad (\text{case III}) \quad (85)$$

with nontrivially modified scaling dimension  $\Delta_\sigma(u)$  that reduces to  $1/8$  at  $u = 0$ . The behavior above could arise, e.g., if the special measurement strings that we explored analytically yield the most important contributions to the numerator in  $r(Z_j Z_k)$ ; the denominator would then compensate for the rarity of these outcomes, thereby boosting the overall scale such that the result remains finite even at  $N \rightarrow \infty$ . For case IV with  $C \neq 0$  we similarly (and more confidently) conjecture that

$$r(Z_j) = f(u) \quad (\text{case IV}) \quad (86)$$

with  $f(u)$  a function that vanishes at  $u = 0$  but is finite at  $N \rightarrow \infty$  when  $u \neq 0$ . Indeed, a finite result when  $N \rightarrow \infty$  for  $r(Z_j)$  seems very plausible given that symmetry does not require the one-point correlator to vanish here.

We performed a numerical experiment of Eqs. (85) and (86) using DMRG, focusing on paramagnetic ancilla. Figure 15 presents the results for  $r(Z_0 Z_j)$  in case III, which indeed reveals power-law decay with scaling dimension exceeding  $1/8$  at  $u > 0$ . In fact, the extrapolated exponents are quite similar to those in Figure 8(c), obtained for case III with a post-selected uniform-string

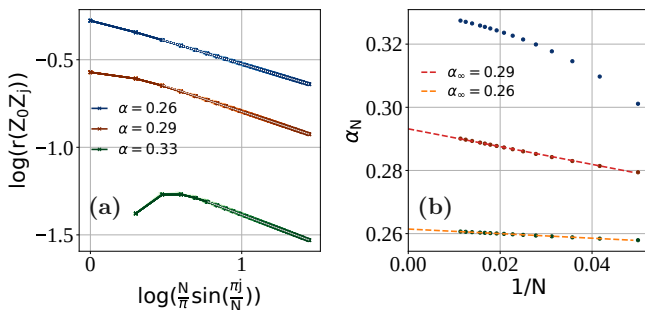


FIG. 15: (Color online). **Ratio  $r(Z_0 Z_j)$  in Eq. (84) involving symmetry-resolved measurement averages.** The data correspond to case III from Table I with paramagnetic ancilla, and different system sizes between  $N = 20$  (light colors in (a)) and  $N = 88$  (dark colors in (a)). At  $u > 0$ , the curves exhibit power-law decay with exponent exceeding  $1/4$ , in agreement with Eq. (85). This tendency continues upon extrapolating to the thermodynamic limit, as shown in (b). Data were obtained using finite DMRG with periodic boundary conditions and bond dimension 1000.

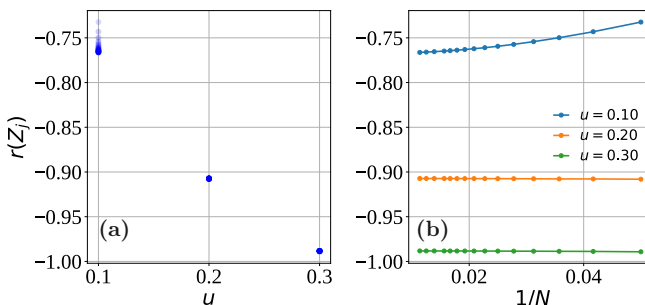


FIG. 16: (Color online). **Ratio  $r(Z_j)$  in Eq. (84) involving symmetry-resolved measurement averages.** The data correspond to case IV from Table I with paramagnetic ancilla,  $C = -1$ , and system sizes between  $N = 20$  (light colors in (a)) and  $N = 88$  (dark colors in (a)). The sizable non-zero value of the ratio generated by  $u \neq 0$  supports Eq. (86). As shown in (b), increasing  $u$  suppresses the dependence on system size such that  $r(Z_j)$  quickly saturates to a finite value. Data were obtained using finite DMRG with periodic boundary conditions and bond dimension 1000.

measurement outcome. Figure 16 reports the results for  $r(Z_j)$  in case IV with non-zero  $C$ . Here too our conjecture is borne out. Even for fairly small  $u = 0.2, 0.3$ ,  $r(Z_j)$  takes on order-one values that, at least for  $u \gtrsim 0.2$ , quickly saturate as  $N$  increases. The  $r(Z_j)$  values are, interestingly, of similar size to  $\langle Z_j \rangle_{\bar{s}}$  extracted for case IV in the uniform post-selection sector [even though the absolute value of  $r(Z_j)$  is not bounded]; cf. Figure 11(b).

## VIII. DISCUSSION AND OUTLOOK

We analyzed the initialize-entangle-measure-probe protocol summarized in Figure 1 to investigate how mea-

surements impact correlations in 1D Ising quantum critical points. Specifically, we developed a perturbative formalism that allowed us to analytically study the outcome of our protocol applied with the four classes of unitaries and projective ancilla measurements listed in Table I. Within this approach, long-distance correlations of microscopic spin operators were related to correlations of low-energy fields evaluated with respect to the usual Ising CFT action perturbed by a ‘defect line’. The detailed structure of the defect line depends on the choice of entangling unitary, the initial ancilla state, and the outcome of ancilla measurements. We argued that, with  $\tilde{Z}$ -basis ancilla measurements, this formalism applies to general measurement outcomes; with  $\tilde{X}$ -basis ancilla measurements, however, well-behaved defect-line actions emerge only for a restricted set of (high-probability) measurement outcomes. In the latter context, we hope that future work can develop a more complete analytic theory capable of treating arbitrary measurement outcomes and assessing their probabilities for general ancilla initializations.

Various predictions follow from this framework—most of which we supported with numerical simulations. We recapitulate our main findings here:

**Case I: unitary  $U_j = e^{iu(X_j - \langle X \rangle) \tilde{X}_j}$ ,  $\tilde{Z}$ -basis measurements.** Non-perturbative CFT results [57] allow one to formally compute the coarse-grained two-point spin correlation function  $\langle Z_j Z_{j'} \rangle_{\bar{s}}$  for general measurement outcomes  $\bar{s}$ . For a uniform measurement outcome—which occurs with highest probability—the two-point function exhibits power-law decay with a measurement-induced change in the scaling dimension. Our formulation also captured subtle changes in correlations that arise with measurement outcomes featuring a domain wall.

**Case II: unitary  $U_j = e^{iu(Z_j - C) \tilde{X}_j}$ ,  $\tilde{Z}$ -basis measurements.** With  $C \neq 0$  the defect-line action includes a longitudinal-field term that explicitly breaks the  $\mathbb{Z}_2$  symmetry enjoyed by the critical chain prior to measurement. Correspondingly, the one-point function  $\langle Z_j \rangle_{\bar{s}}$  becomes non-zero, with a spatial profile dependent on the measurement outcome. Averaging  $\langle Z_j \rangle_{\bar{s}}$  over measurement outcomes yields a vanishing one-point function as required on general grounds. By contrast, averaging  $\langle Z_j \rangle_{\bar{s}}^2$  retains memory of the measurements and yields a non-zero result that, based on our exact diagonalization results, appears to survive in the thermodynamic limit.

**Case III: unitary  $U_j = e^{iu(X_j - \langle X \rangle) \tilde{Z}_j}$ ,  $\tilde{X}$ -basis measurements.** Just as for case I, the uniform string measurement outcome occurs with highest probability and yields a two-point function  $\langle Z_j Z_{j'} \rangle_{\bar{s}}$  with modified scaling dimension.

**Case IV: unitary  $U_j = e^{iu(Z_j - C) \tilde{Z}_j}$ ,  $\tilde{X}$ -basis measurements.** As for case II, explicit breaking of  $\mathbb{Z}_2$  symmetry induced by  $C \neq 0$  yields a non-zero one-point function  $\langle Z_j \rangle_{\bar{s}}$  for the nearly uniform measurement outcomes amenable to our perturbative formalism. Taking  $C = 0$  restores  $\mathbb{Z}_2$  symmetry for the critical chain. Here,

when the ancilla are *also* critical, the defect-line action hosts a long-range power-law decaying interaction among CFT spin-fields that, based on iDMRG simulations, appears to suppress  $\langle Z_j Z_{j'} \rangle_{\tilde{s}}$  correlations in a manner that yields faster-than-power-law decay (for uniform or nearly uniform measurement outcomes). That is, within this post-selection sector, arbitrarily weak entangling gates followed by ancilla measurements potentially obliterate critical correlations in the chain, despite the absence of explicit symmetry breaking. Further substantiating this scenario, possibly drawing connections to previous work on long-range-interacting Ising chains [58], raises an interesting open problem.

In the cases with  $\tilde{X}$ -basis ancilla measurements, we further proposed a new method for detecting non-trivial effects of measurements on Ising quantum criticality that altogether eschews the requirement of post-selection. Here we exploited the fact that  $\tilde{X}$ -basis measurement outcomes factorize into two symmetry sectors depending on the value of the generator  $\tilde{G} = \prod_j \tilde{X}_j \in \pm 1$  of the global  $\mathbb{Z}_2$  symmetry for the ancilla. Although  $\tilde{G}$  is a non-local operator, its eigenvalue for any outcome  $|\tilde{s}\rangle$  follows trivially given measurements of  $\tilde{X}_j$  for each ancilla site; one can, in turn, average critical-chain observables over measurement outcomes separately within each symmetry sector. We conjectured that the *difference* in averages between the two sectors (normalized by the difference in probability for accessing the sectors) encodes measurement effects on Ising criticality that survive in the thermodynamic limit. Strikingly, our simulations of this ratio for one- and two-point spin correlations indeed mimic the behavior predicted for uniform post-selection outcomes by our perturbative defect-line framework. The practical catch is that the ratio involves a numerator and denominator that individually decay to zero as the system size increases. It would thus be valuable to understand the effects of measurement errors and decoherence on this quantity to address its suitability for experimental application. More broadly, might analogous factorization into symmetry sectors prove useful for taming the post-selection problem in other measurement-induced phenomena?

In much of this work, correlations in the initialized ancilla state played an important role. Cases I and II, for instance, become completely trivial if the ancilla are initialized into the (product-state) ground state of Eq. (14) at  $h_{\text{anc}}/J_{\text{anc}} \rightarrow \infty$ . In this extreme case  $|\psi_a\rangle$  is an eigenstate of the  $U_j$ 's used in our protocol for cases I and II. Hence those unitaries do not actually entangle the critical chain with the ancilla, and measurements of the latter do not affect the former. Case IV highlights a more striking example, where once again critical ancilla can produce a defect-line action exhibiting inherently long-range interaction among CFT fields, mediating physics qualitatively different from what we found with paramagnetic ancilla.

Outside of this last example, we invariably concluded that the defect-line action could be approximated by a single term linear in either the  $\sigma$  or  $\varepsilon$  field (depending

on the protocol details under consideration). Microscopically, we showed that for the post-measurement state  $|\psi_{\tilde{s}}\rangle = \frac{1}{\sqrt{N}} U' e^{-H_m/2} |\psi_c\rangle$  [Eq. (22)], the important non-unitary  $e^{-H_m/2}$  part generically does not factorize into a product of operators acting at individual sites  $j$  due to the  $V_{jk}$  term in Eq. (34). An approximate factorized form,

$$|\psi_{\tilde{s}}\rangle \approx \frac{1}{\sqrt{p_{\tilde{s}}}} \prod_j M_j |\psi_c\rangle, \quad (87)$$

nevertheless captures the leading defect-line action linear in  $\sigma$  or  $\varepsilon$  that we typically obtained. When  $m_j$  is non-zero, the factorized measurement operators  $M_j$  follow by simply setting  $V_{jk} = 0$  in  $H_m$ ; with  $m_j = 0$ , one instead modifies the  $V_{jk}$  term by ‘fusing’ the constituent microscopic operators (mimicking the CFT-field fusion rules) to arrive at a factorizable form. Intuitively, the more highly entangled the ancilla are, the worse this approximation becomes—culminating in its complete breakdown in case IV with  $C = 0$  when the ancilla are critical. It would be interesting to quantify the accuracy of Eq. (87) from a microscopic viewpoint, e.g., by studying the operator space entanglement of  $M_{\tilde{s}}$  as a function of the ancilla wavefunction.

Chains of laser-excited Rydberg atoms trapped in optical tweezer arrays comprise a promising experimental platform for measurement-altered Ising criticality. A single Rydberg chain effectively realizes an antiferromagnetic spin model with power-law-decaying Ising interactions, supplemented by both transverse *and* longitudinal fields—though the latter can be tuned to zero by choosing an appropriate detuning from resonance. The phase diagram hosts a readily accessible Ising quantum phase transition (among other more exotic critical points) [59] that is well-understood also at the lattice level in this setting [48]. Moreover, a second Rydberg chain could furnish the ancilla degrees of freedom in our protocol. Devising concrete implementations of the requisite unitaries and ancilla measurements in this venue poses a nontrivial problem for future work. Additionally, the pursuit of measurement-altered criticality in Rydberg arrays highlights several fundamental open questions—including the impact of antiferromagnetic Ising interactions, a non-zero longitudinal field, integrability-breaking perturbations, etc.

Finally, many other variations on the present work would be interesting to explore. Extension to strongly interacting CFTs—e.g., tricritical Ising, parafermionic, etc.—is particularly intriguing given their rich field content, and correspondingly rich set of possible measurement-induced defect-line actions. Measurements could also be performed in various alternative ways that add a new twist into the problem; for instance, one could contemplate joint measurements of operators on the critical and ancilla chains, or measure different quantities in different regions of space. We hope that the approach used here will prove useful for addressing such problems in the future.

*Note added:* While finishing this work we became aware of Refs. 60, 61, which examined the effects of measurement on Ising criticality from a perspective largely complementary to ours.

### Acknowledgments

It is a pleasure to acknowledge enlightening conversations with Ehud Altman, Manuel Endres, Matthew Fisher, Sheng-Hsuan Lin, and Omar Wani. Tensor network calculations were performed using the TeNPy Li-

brary [51]. The U.S. Department of Energy, Office of Science, National Quantum Information Science Research Centers, Quantum Science Center supported the construction and numerical analysis of the protocol for probing measurement-altered Ising criticality. Additional support was provided by the National Science Foundation through grant DMR-1848336 (RM); the Caltech Institute for Quantum Information and Matter, an NSF Physics Frontiers Center with support of the Gordon and Betty Moore Foundation through Grant GBMF1250; and the Walter Burke Institute for Theoretical Physics at Caltech.

## Appendix A: Gaussian overlaps

Throughout the manuscript, we are interested in the evaluation of correlation functions like the ones appearing in Eq. (31). To fix the ideas, we focus on the case in which we have  $\tilde{X}$  in the unitary, we measure in the  $z$ -basis and we want to evaluate

$$a(i_1, \dots, i_{N_F}) = \frac{\langle \tilde{s} | \prod_{j=1}^{N_F} \tilde{X}_{i_j} | \psi_a \rangle}{\langle \tilde{s} | \psi_a \rangle}, \quad (\text{A1})$$

where  $\tilde{s}$  is an arbitrary string outcome and  $N_F$  is the number of flipped spins.  $|\psi_a\rangle$  is the ground state of the transverse field Ising model in Eq. (1) or, equivalently, of Eq. (3). We can collect the Majorana operators in the vector  $\vec{\gamma}$

$$\vec{\gamma} = \begin{pmatrix} \gamma_{A,1} \\ \gamma_{A,2} \\ \vdots \\ \gamma_{A,N} \\ \gamma_{B,1} \\ \vdots \\ \gamma_{B,N} \end{pmatrix}, \quad (\text{A2})$$

where  $N$  is the system size, and  $\{\vec{\gamma}_i, \vec{\gamma}_j\} = 2\delta_{ij}$ . The Hamiltonian is quadratic in the fermionic operators and any fermionic Gaussian state can be described through the covariance matrix defined as

$$\Gamma_{jk} = \frac{i}{2} \langle [\gamma_j, \gamma_k] \rangle, \quad (\text{A3})$$

with  $[\gamma_j, \gamma_k]$  the commutator of the two Majorana operators  $\gamma_j$  and  $\gamma_k$ . From the definition, we observe that  $\Gamma$  is a real and skew-symmetric matrix. For the transverse field Ising chain, the covariance matrix is known analytically [62]. In particular it has a Toeplitz structure given by

$$\Gamma_{jk} = \frac{1}{N} \sum_{k \in \Omega_{\text{gs}}} e^{\frac{2\pi i k}{N}(j-k)} \begin{pmatrix} 0 & \frac{1 - \cos(\frac{2\pi k}{N}) + i \sin(\frac{2\pi k}{N})}{\sqrt{2 - 2 \cos(\frac{2\pi k}{N})}} \\ \frac{1 - \cos(\frac{2\pi k}{N}) + i \sin(\frac{2\pi k}{N})}{\sqrt{2 - 2 \cos(\frac{2\pi k}{N})}} & 0 \end{pmatrix}, \quad (\text{A4})$$

where  $\Omega_{\text{gs}}$  is the set of occupied momenta in the ground state. We can also use an alternative approach to determine the covariance matrix. We can rewrite Eq. (3) as  $H = \frac{1}{2} \sum_{j,k} h_{jk} \gamma_j \gamma_k$ , where now  $h$  is the single-particle Hamiltonian. We proceed by first finding the fermionic transformation  $U$  that diagonalize  $h$  and in this diagonal basis the correlation matrix associated to the ground state,  $\Gamma_{\text{diag}}$ , is simply obtained by replacing  $-1$  ( $1$ ) for any positive (negative) eigenvalue [63]. To obtain  $\Gamma$ , we just need to move back to the original basis, i.e.  $\Gamma = U^\dagger \Gamma_{\text{diag}} U$ .

When we measure in the  $z$ -basis,  $|\tilde{s}\rangle$  is not a Gaussian state, but noticing that  $\langle \tilde{s} | \tilde{X}_j | \psi_a \rangle = \langle \tilde{s} | \tilde{X}_j \tilde{G} | \psi_a \rangle = \langle -\tilde{s} | \tilde{X}_j | \psi_a \rangle$ , we find

$$\langle \tilde{s} | \tilde{X}_j | \psi_a \rangle = \frac{1}{\sqrt{2}} \langle \psi_+ | \tilde{X}_j | \psi_a \rangle, \quad |\psi_+\rangle = \frac{|\tilde{s}\rangle + |-\tilde{s}\rangle}{\sqrt{2}}. \quad (\text{A5})$$

The advantage of using the cat state  $|\psi_+\rangle$  is that now it is Gaussian and it corresponds to the ground state of a quadratic Hamiltonian

$$H_{\{\tilde{s}\}} = - \sum_j \tilde{s}_j \tilde{s}_{j+1} \tilde{Z}_j \tilde{Z}_{j+1}, \quad (\text{A6})$$

that after a Jordan-Wigner transformation reads

$$H_{\{\tilde{s}\}} = i \sum_j \tilde{s}_j \tilde{s}_{j+1} \gamma_{A,j+1} \gamma_{B,j} \equiv \frac{1}{2} \sum_{jk} h_{jk}^{\{\tilde{s}\}} \gamma_j \gamma_k. \quad (\text{A7})$$

By applying the procedure described above, we can find the covariance matrix describing the Gaussian ground state of Eq. (A7),  $\Gamma_{\{\tilde{s}\}}$ . Once we know the covariance matrix both for the ground state of the Ising ancillary system and for the Hamiltonian  $H_{\{\tilde{s}\}}$ , we can apply a result found in Ref. [54]: the absolute value of the inner product  $\langle \tilde{s} | \psi_a \rangle$  is

$$|\langle \tilde{s} | \psi_a \rangle| = \sqrt{2^{-N-1} \text{Pf}(\Gamma + \Gamma_{\{\tilde{s}\}})}, \quad (\text{A8})$$

where Pf is the Pfaffian of  $\Gamma + \Gamma_{\{\bar{s}\}}$ . If we are interested in the evaluation of Eq. (A1), since  $\{\bar{s}\}$  is an eigenstate of  $\prod_j \tilde{X}_{i_j}$ , we can apply it on  $\langle \bar{s} |$ , modify the string outcome, the Hamiltonian  $H_{\{\bar{s}\}}$  and the correlation function can be still computed using Eq. (A8). For example,  $a(j)$  and  $a(j, k)$  in Eqs. (35) are given by

$$a(j) = \sqrt{\frac{\text{Pf}(\Gamma + \Gamma_{\tilde{X}_{j, \{\bar{s}\}}})}{\text{Pf}(\Gamma + \Gamma_{\{\bar{s}\}})}}, \quad a(j, k) = \sqrt{\frac{\text{Pf}(\Gamma + \Gamma_{\tilde{X}_{j, k, \{\bar{s}\}}})}{\text{Pf}(\Gamma + \Gamma_{\{\bar{s}\}})}}, \quad (\text{A9})$$

where  $\tilde{X}_{j, k, \{\bar{s}\}}$  denotes the string outcome after having applied  $\tilde{X}$  on the  $j, k$ -th sites. It is relevant to comment that the absolute value in Eq. (A8) is superfluous for the model we are considering in this manuscript due to the stoquasticity of the transverse field Ising model.

When we measure in the  $x$ -basis, now  $|\bar{s}\rangle$  is a Gaussian state, describing the ground state of the quadratic Hamiltonian

$$H_{\bar{s}} = - \sum_j \tilde{s}_j \tilde{X}_j \longrightarrow -i \sum_j \tilde{s}_j \gamma_{A, j} \gamma_{B, j}. \quad (\text{A10})$$

Therefore, computing the corresponding covariance matrix, we can apply again Eq. (A8) to evaluate

$$\langle \bar{s} | \psi_a \rangle = \sqrt{2^{-N} \text{Pf}(\Gamma + \Gamma_{\bar{s}})}, \quad (\text{A11})$$

and also correlation functions like  $\frac{\langle \bar{s} | \prod_{j=1}^{N_F} \tilde{Z}_{i_j} | \psi_a \rangle}{\langle \bar{s} | \psi_a \rangle}$ .

- 
- [1] Y. Li, X. Chen, and M. P. A. Fisher, Phys. Rev. B **98**, 205136 (2018), URL <https://link.aps.org/doi/10.1103/PhysRevB.98.205136>.
- [2] B. Skinner, J. Ruhman, and A. Nahum, Phys. Rev. X **9**, 031009 (2019), URL <https://link.aps.org/doi/10.1103/PhysRevX.9.031009>.
- [3] Y. Li, X. Chen, and M. P. A. Fisher, Phys. Rev. B **100**, 134306 (2019), URL <https://link.aps.org/doi/10.1103/PhysRevB.100.134306>.
- [4] A. Chan, R. M. Nandkishore, M. Pretko, and G. Smith, Phys. Rev. B **99**, 224307 (2019), URL <https://link.aps.org/doi/10.1103/PhysRevB.99.224307>.
- [5] M. J. Gullans and D. A. Huse, Phys. Rev. X **10**, 041020 (2020), URL <https://link.aps.org/doi/10.1103/PhysRevX.10.041020>.
- [6] S. Choi, Y. Bao, X.-L. Qi, and E. Altman, Phys. Rev. Lett. **125**, 030505 (2020), URL <https://link.aps.org/doi/10.1103/PhysRevLett.125.030505>.
- [7] C.-M. Jian, Y.-Z. You, R. Vasseur, and A. W. W. Ludwig, Phys. Rev. B **101**, 104302 (2020), URL <https://link.aps.org/doi/10.1103/PhysRevB.101.104302>.
- [8] O. Alberton, M. Buchhold, and S. Diehl, Phys. Rev. Lett. **126**, 170602 (2021), URL <https://link.aps.org/doi/10.1103/PhysRevLett.126.170602>.
- [9] A. Biella and M. Schiró, Quantum **5**, 528 (2021), URL <https://doi.org/10.22331/q-2021-08-19-528>.
- [10] X. Turkeshi, L. Piroli, and M. Schiró, Phys. Rev. B **106**, 024304 (2022), URL <https://link.aps.org/doi/10.1103/PhysRevB.106.024304>.
- [11] X. Cao, A. Tilloy, and A. D. Luca, SciPost Phys. **7**, 024 (2019), URL <https://scipost.org/10.21468/SciPostPhys.7.2.024>.
- [12] M. J. Gullans and D. A. Huse, Phys. Rev. Lett. **125**, 070606 (2020), URL <https://doi.org/10.1103/physrevlett.125.070606>.
- [13] Y. Bao, S. Choi, and E. Altman, Phys. Rev. B **101**, 104301 (2020), URL <https://link.aps.org/doi/10.1103/PhysRevB.101.104301>.
- [14] T. Boorman, M. Szyniszewski, H. Schomerus, and A. Romito, Phys. Rev. B **105**, 144202 (2022), URL <https://link.aps.org/doi/10.1103/PhysRevB.105.144202>.
- [15] R. Fan, S. Vijay, A. Vishwanath, and Y.-Z. You, Phys. Rev. B **103**, 174309 (2021), URL <https://link.aps.org/doi/10.1103/PhysRevB.103.174309>.
- [16] G. S. Bentsen, S. Sahu, and B. Swingle, Phys. Rev. B **104**, 094304 (2021), URL <https://link.aps.org/doi/10.1103/PhysRevB.104.094304>.
- [17] Y. Li, X. Chen, A. W. W. Ludwig, and M. P. A. Fisher, Phys. Rev. B **104**, 104305 (2021), URL <https://link.aps.org/doi/10.1103/PhysRevB.104.104305>.
- [18] A. J. Friedman, C. Yin, Y. Hong, and A. Lucas, *Locality and error correction in quantum dynamics with measurement* (2022), 2206.09929.
- [19] X. Turkeshi, R. Fazio, and M. Dalmonte, Phys. Rev. B **102**, 014315 (2020), URL <https://link.aps.org/doi/10.1103/PhysRevB.102.014315>.
- [20] X. Turkeshi, A. Biella, R. Fazio, M. Dalmonte, and M. Schiró, Phys. Rev. B **103**, 224210 (2021), URL <https://link.aps.org/doi/10.1103/PhysRevB.103.224210>.
- [21] T. Müller, S. Diehl, and M. Buchhold, Phys. Rev. Lett. **128**, 010605 (2022), URL <https://link.aps.org/doi/10.1103/PhysRevLett.128.010605>.
- [22] A. Lavasani, A. Y., and M. Maissam Barkeshli, Nat.Phys. **17**, 342–347 (2021), URL <https://www.nature.com/articles/s41567-022-01619-7>.
- [23] Y. Bao, S. Choi, and E. Altman, Ann. of Phys. **435**, 168618 (2021), URL <https://www.sciencedirect.com/science/article/pii/S0003491621002244>.
- [24] M. Van Regemortel, Z.-P. Cian, A. Seif, H. De-

- hghani, and M. Hafezi, Phys. Rev. Lett. **126**, 123604 (2021), URL <https://link.aps.org/doi/10.1103/PhysRevLett.126.123604>.
- [25] M. Ippoliti, M. J. Gullans, S. Gopalakrishnan, D. A. Huse, and V. Khemani, Phys. Rev. X **11**, 011030 (2021), URL <https://link.aps.org/doi/10.1103/PhysRevX.11.011030>.
- [26] L. Piroli, G. Styliaris, and J. I. Cirac, Phys. Rev. Lett. **127**, 220503 (2021), URL <https://link.aps.org/doi/10.1103/PhysRevLett.127.220503>.
- [27] R. Verresen, N. Tantivasadakarn, and A. Vishwanath, *Efficiently preparing schrodinger's cat, fractons and non-abelian topological order in quantum devices* (2021), 2112.03061.
- [28] N. Tantivasadakarn, R. Thorngren, A. Vishwanath, and R. Verresen, *Long-range entanglement from measuring symmetry-protected topological phases* (2021), 2112.01519.
- [29] N. Tantivasadakarn, A. Vishwanath, and R. Verresen, *A hierarchy of topological order from finite-depth unitaries, measurement and feedforward* (2022), 2209.06202.
- [30] T.-C. Lu, L. A. Lessa, I. H. Kim, and T. H. Hsieh, *Measurement as a shortcut to long-range entangled quantum matter* (2022), 2206.13527.
- [31] S. Bravyi, I. Kim, A. Kliesch, and R. Koenig, *Adaptive constant-depth circuits for manipulating non-abelian anyons* (2022), 2205.01933.
- [32] G.-Y. Zhu, N. Tantivasadakarn, A. Vishwanath, S. Trebst, and R. Verresen, *Nishimori's cat: stable long-range entanglement from finite-depth unitaries and weak measurements* (2022), 2208.11136.
- [33] J. Y. Lee, W. Ji, Z. Bi, and M. P. A. Fisher, *Decoding measurement-prepared quantum phases and transitions: from ising model to gauge theory, and beyond* (2022), 2208.11699.
- [34] C. Noel, P. Niroula, A. Zhu, Dand Risinger, L. Egan, D. Biswas, M. Cetina, A. V. Gorshkov, M. J. Gullans, D. A. Huse, and C. Monroe, Nat. Phys. **18**, 760–764 (2022), URL <https://doi.org/10.1038/s41567-022-01619-7>.
- [35] J. M. Koh, S.-N. Sun, M. Motta, and A. J. Minnich, *Experimental realization of a measurement-induced entanglement phase transition on a superconducting quantum processor* (2022), 2203.04338.
- [36] M. Iqbal, N. Tantivasadakarn, T. M. Gatterman, J. A. Gerber, K. Gilmore, D. Gresh, A. Hankin, N. Hewitt, C. V. Horst, M. Matheny, et al., *Topological order from measurements and feed-forward on a trapped ion quantum computer* (2023), 2302.01917.
- [37] H. Dehghani, A. Lavasani, M. Hafezi, and M. J. Gullans, *Neural-network decoders for measurement induced phase transitions* (2022), 2204.10904.
- [38] M. Ippoliti and V. Khemani, Phys. Rev. Lett. **126**, 060501 (2021), URL <https://link.aps.org/doi/10.1103/PhysRevLett.126.060501>.
- [39] M. Ippoliti, T. Rakovszky, and V. Khemani, Phys. Rev. X **12**, 011045 (2022), URL <https://link.aps.org/doi/10.1103/PhysRevX.12.011045>.
- [40] T.-C. Lu and T. Grover, PRX Quantum **2**, 040319 (2021), URL <https://link.aps.org/doi/10.1103/PRXQuantum.2.040319>.
- [41] Y. Li, Y. Zou, P. Glorioso, E. Altman, and M. P. A. Fisher, *Cross entropy benchmark for measurement-induced phase transitions* (2022), 2209.00609.
- [42] S. J. Garratt, Z. Weinstein, and E. Altman, *Measurements conspire nonlocally to restructure critical quantum states* (2022), 2207.09476.
- [43] C. L. Kane and M. P. A. Fisher, Phys. Rev. Lett. **68**, 1220 (1992), URL <https://link.aps.org/doi/10.1103/PhysRevLett.68.1220>.
- [44] X. Sun, H. Yao, and S.-K. Jian, *New critical states induced by measurement* (2023), 2301.11337.
- [45] J. Y. Lee, C.-M. Jian, and C. Xu, *Quantum criticality under decoherence or weak measurement* (2023), 2301.05238.
- [46] Y. Bao, R. Fan, A. Vishwanath, and E. Altman, *Mixed-state topological order and the errorfield double formulation of decoherence-induced transitions* (2023), 2301.05687.
- [47] R. Fan, Y. Bao, E. Altman, and A. Vishwanath, *Diagnostics of mixed-state topological order and breakdown of quantum memory* (2023), 2301.05689.
- [48] K. Slagle, D. Aasen, H. Pichler, R. S. K. Mong, P. Fendley, X. Chen, M. Endres, and J. Alicea, Phys. Rev. B **104**, 235109 (2021), URL <https://link.aps.org/doi/10.1103/PhysRevB.104.235109>.
- [49] P. Di Francesco, P. Mathieu, and D. Senechal, *Conformal Field Theory* (1997).
- [50] M. A. Nielsen and I. L. Chuang, *Quantum Computation and Quantum Information: 10th Anniversary Edition* (Cambridge University Press, USA, 2011), 10th ed., ISBN 1107002176.
- [51] J. Hauschild and F. Pollmann, SciPost Phys. Lect. Notes p. 5 (2018), code available from <https://github.com/tenpy/tenpy>, 1805.00055, URL <https://scipost.org/10.21468/SciPostPhysLectNotes.5>.
- [52] S. R. White, Phys. Rev. Lett. **69**, 2863 (1992), URL <https://link.aps.org/doi/10.1103/PhysRevLett.69.2863>.
- [53] I. P. McCulloch, *Infinite size density matrix renormalization group, revisited* (2008), 0804.2509.
- [54] S. Bravyi, D. P. Divincenzo, R. Oliveira, and B. M. Terhal, Quantum Info. Comput. **8**, 361–385 (2008), URL <https://dl.acm.org/doi/10.5555/2011772.2011773>.
- [55] B. M. McCoy and J. H. H. Perk, Phys. Rev. Lett. **144**, 840 (1980), URL <https://link.aps.org/doi/10.1103/PhysRevLett.44.840>.
- [56] D. Cabra and C. Naó, Mod. Phys. Lett. A **09**, 2017 (1994), URL <https://doi.org/10.1142/s0217732394001969>.
- [57] C. Naó n and M. Trobo, J. Stat. Mech. **2011**, P02021 (2011), URL <https://doi.org/10.1088/1742-5468/2011/02/p02021>.
- [58] T. Koffel, M. Lewenstein, and L. Tagliacozzo, Phys. Rev. Lett. **109**, 267203 (2012), URL <https://link.aps.org/doi/10.1103/PhysRevLett.109.267203>.
- [59] P. Fendley, K. Sengupta, and S. Sachdev, Phys. Rev. B **69**, 075106 (2004), URL <https://link.aps.org/doi/10.1103/PhysRevB.69.075106>.
- [60] Z. Weinstein, R. Sajith, E. Altman, and S. J. Garratt, *Nonlocality and entanglement in measured critical quantum ising chains* (2023), 2301.08268.
- [61] Z. Yang, D. Mao, and C.-M. Jian, *Entanglement in one-dimensional critical state after measurements* (2023), 2301.08255.
- [62] J. I. Latorre, E. Rico, and G. Vidal, Quantum Info. Comput. **4**, 48–92 (2004), URL <https://arxiv.org/abs/quant-ph/0304098>.

- [63] J. Surace and L. Tagliacozzo, SciPost Phys. Lect. Notes **54** (2022), URL <https://doi.org/10.21468/scipostphyslectnotes.54>.
- [64] Notice that  $\langle i\gamma_R\gamma_L \rangle = 0$  when evaluated in the critical Ising CFT
- [65] Otherwise the measurement translates into a control unitary on the top chain depending on the measurement outcome of the bottom chain.
- [66] The high probability of this measurement outcome becomes intuitive in the  $h_{\text{anc}}/J_{\text{anc}} \gg 1$  regime.
- [67] Explicitly, after dropping terms that vanish by time-reversal symmetry, one finds  $\langle (U')^\dagger Z_j Z_{j'} U' \rangle_{\bar{s}} = \cos(2ua(j)) \cos(2ua(j')) \langle Z_j Z_{j'} \rangle_{\bar{s}} + \sin(2ua(j)) \sin(2ua(j')) \langle Y_j Y_{j'} \rangle_{\bar{s}}$ . Given that (i)  $Y_j$  maps to a CFT operator with larger scaling dimension than that for  $Z_j$  and (ii) our perturbative expansion focuses on the  $u \ll 1$  regime, the  $U'$  unitary can be safely neglected.